SRESA's International Journal of

LIFE CYCLE RELIABILITY AND SAFETY ENGINEERING

Vol.5 **Issue No.2** **April–June 2016** **ISSN – 2250 0820**

Special Issue on

"CURRENT TRENDS IN RELIABILITY: INDUSTRIAL APPLICATIONS"

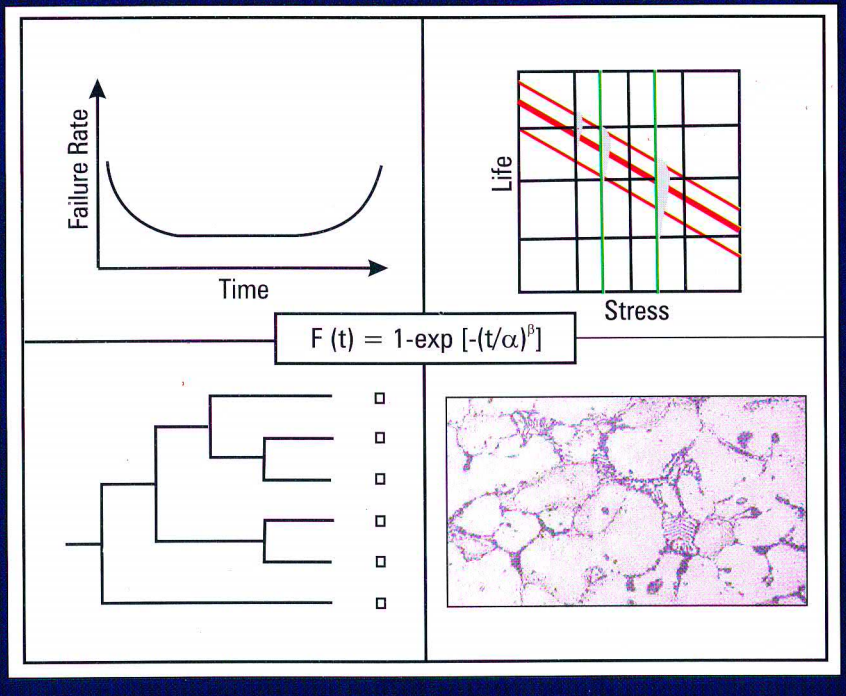

Guest Editor:
Dr. C. Senthil Kur
Dr. R. Muthukun

Chief-Editors

P.V. Varde
A.K. Verma
Michael G. Pecht

Society for Reliability and Safety

website: http://www.sresa.org.in

SRESA Journal of Life Cycle Reliability and Safety Engineering

Extensive work is being performed world over on assessment of Reliability and Safety for engineering systems in support of decisions. The increasing number of risk-based / risk-informed applications being developed world over is a testimony to the growth of this field. Here, along with probabilistic methods, deterministic methods including Physics-of-Failure based approach is playing an important role. The International Journal of Life Cycle Reliability and Safety Engineering provides a unique medium for researchers and academicians to contribute articles based on their R&D work, applied work and review work, in the area of Reliability, Safety and related fields. Articles based on technology development will also be published as Technical Notes. Review articles on Books published in the subject area of the journal will also form part of the publication.

Society for Reliability and Safety has been actively working for developing means and methods for improving system reliability. Publications of quarterly News Letters and this journal are some of the areas the society is vigorously pursuing for societal benefits. Manuscript in the subject areas can be communicated to the Chief Editors. Manuscript will be reviewed by the experts in the respective area of the work and comments will be communicated to the corresponding author. The reviewed final manuscript will be published and the author will be communicated the publication details. Instruction for preparing the manuscript has been given on inside page of the end cover page of each issue. The rights of publication rest with the Chief-Editors.

SCOPE OF JOURNAL

System Reliability analysis	Structural Reliability	Risk-based applications
Statistical tools and methods	Remaining life prediction	Technical specification optimization
Probabilistic Safety Assessment	Reliability based design	Risk-informed approach
Quantitative methods	Physics-of-Failure methods	Risk-based ISI
Human factor modeling	Probabilistic Fracture Mechanics	Risk-based maintenance
Common Cause Failure analysis	Passive system reliability	Risk-monitor
Life testing methods	Precursor event analysis	Prognostics & health management
Software reliability	Bayesian modeling	Severe accident management
Uncertainty modeling	Artificial intelligence in risk and reliability modeling	Risk-based Operator support systems
Dynamic reliability models	Design of Experiments	Role of risk-based approach in Regulatory reviews
Sensitivity analysis	Fuzzy approach in risk analysis	Advanced electronic systems reliability modeling
Decision support systems	Cognitive framework	Risk-informed asset management

SRESA AND ITS OBJECTIVES

a) To promote and develop the science of reliability and safety.

b) To encourage research in the area of reliability and safety engineering technology & allied fields.

c) To hold meetings for presentation and discussion of scientific and technical issues related to safety and reliability.

d) To evolve a unified standard code of practice in safety and reliability engineering for assurance of quality based professional engineering services.

e) To publish journals, books, reports and other information, alone or in collaboration with other organizations, and to disseminate information, knowledge and practice of ensuring quality services in the field of Reliability and Safety.

f) To organize reliability and safety engineering courses and / or services for any kind of energy systems like nuclear and thermal power plants, research reactors, other nuclear and radiation facilities, conventional process and chemical industries.

g) To co-operate with government agencies, educational institutions and research oganisations

SRESA's International Journal of

LIFE CYCLE RELIABILITY AND SAFETY ENGINEERING

Vol.5 Issue No.2 April–June 2016 ISSN – 2250 0820

Special Issue on

"CURRENT TRENDS IN RELIABILITY: INDUSTRIAL APPLICATIONS"

Guest Editor:
Dr. C. Senthil Kumar
Dr. R. Muthukumar

SOCIETY FOR RELIABILITY AND SAFETY

Typeset & Printed

EBENEZER PRINTING HOUSE
Unit No. 5 & 11, 2nd Floor, Hind Services Industries,
Veer Savarkar Marg,
Dadar (west), Mumbai -28
Tel.: 2446 2632/ 3872
E-mail: outwork@gmail.com

Guest Editorial

The advances in technology and increasing automation necessitate more focus on ensuring dependability of systems used in critical applications. This is important in view of the consequences to human life and environment during system failures. Further,the need for higher reliability and safety is emphasized due to factors like increased product complexity; public awareness; cost of failure, damage and warranty; safety considerations with undesirable consequences. Reliability and safety engineering has wide applications in all conventional engineering fields. With advanced research, phenomenal progress has been achieved to study, characterize, measure, and analyze the failure, repair, and reduce the consequences of failure thus improving the operational use by increasing their design life. Eliminating or reducing the likelihoods of failures thereby increasing available operating time lead to large scale reduction in downtime. For any safety critical applications such as space, nuclear, medical, etc., reliability and safety play an important role right from conception, design and operational phases.

In this context, considering the importance and relevance of the topic, Society for Reliability and Safety (SRESA) organized series of International conferences, i.e, ICRESH-2005 & 2010 in Mumbai and ICRESH-ARMS-2015 in Sweden addressing reliability and safety in various disciplines of computer science, mechanical engineering, electrical and electronics engineering, electronics and communication engineering, industrial and safety engineering, etc. In 2014, SRESA along with Anna University, BIT Campus, Trichy organized the first national conference NCRS-2014. The conference was attended by students from all over Tamilnadu and distinguished experts form reputed academic institutes and research organizations delivered the lectures.

To provide a platform for scientific deliberations on this important topic, the 2nd National Conference on Reliability and Safety Engineering (NCRS-2015) was organized during October 8-10, 2015, in Anna University, Chennai, Tamilnadu. The scope of the conference included a wide range of topics in reliability. Some of them are component reliability and quality, system and product reliability, accelerated life testing, risk assessment, software reliability, role of six sigma, influence of ageing effects, etc.

This issue of the Journal on Life Cycle Reliability and Safety Engineering are dedicated to NCRS-2015 and five selected peer-reviewed papers are included for publication.

The first paper presents the optimization of process parameters of Orbital TIG welding of 6mm propellant feed tubes made of 304L Stainless Steel material for satellite system using statistical optimization techniques. In this paper, Taguchi linear model analysis of Signal to Noise (SN) ratio and means versus input parameters were carried out. It is observed that the most important parameter affecting the weld quality is welding current.

The second paper reports a procedure to predict the rain fall estimate for longer period from the limited period historical records available. Three statistical distributions, such as Gumbel distribution, power law, and exponential distribution is used for the prediction. The predicted rain fall from these models has large variations and its physical basis are being studied further.

In the third paper, a procedure to estimate the wave run up heights on the shore for various return periods is given. The study includes the local bathymetry into the model using work-energy theorem to improve the prediction of mean run up height.

The fourth paper deals with prediction of remaining useful life of electrolytic capacitors using physics of failure approach and provide an accurate degradation model. Electrolytic capacitors are one of the important devices in various power electronics systems, such as motor drives, uninterruptible

power supply, electric vehicles and dc power supply and form an integral part of many other electronic devices.

The fifth paper estimates the reliability and availability for m/n:G standby system using fourth order Runge-Kutta algorithm with discussion on case studies.

In view of the growing importance of automation in almost every walk of life, ensuring reliability and safety throughout the life cycle of the engineering systems including prediction of future behaviour is vital and to this extent in our view the contents of this journal broadly fulfils.

C. Senthil Kumar
Guest Editor

R. Muthukumar
Guest Editor

Dr. C. Senthil Kumar *has more than 25 years in Indian Atomic Energy Regulatory Board (AERB) and is presently Head of Risk Assessment and GIS section of AERB-Safety Research Institute at Kalpakkam. His areas of specialization include: Reliability Engineering, Risk Assessment studies, Probabilistic Safety Assessment, Software reliability, Seismic Safety, Statistical analysis, etc.*

He was involved in the Level-1 probabilistic safety assessment of Prototype Fast Breeder reactor, specifically in the reliability analysis of shutdown system, decay heat removal system, power supply system and in Passive system reliability analysis. He has significant contribution in the seismic re-evaluation of Fast Breeder Test Reactor at Kalpakkam. His post-doctoral study is in the area of Software reliability for computer based systems in safety critical operations, real-time scheduling for adaptive fault tolerance in multiprocessor systems, software testing, fault injection and mutation studies. He is a member of NEA's Working Group, WG-RISK on Multi-Unit PSA.

After his Ph.D. in Reliability from Anna University in 2005, he did his post-doctoral research at Sweden in 2009-10. He has provided guidance to 3 Ph.D. students, two MS students and several research fellows. He is a recognised supervisor for Ph.D. at Anna University and Bharathiar University and is a member of three doctoral committees of Anna University. He is a reviewer of journal articles in Elsevier publications and has authored / co-authored more than 22 international peer-reviewed journal publications and several national publications. He has received AERB Group achievement award for his contribution to Seismic Re-evaluation of FBTR.

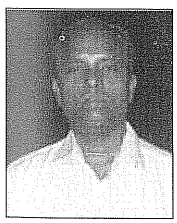

Dr. R. Muthukumar *is a Scientist in Centre for Reliability (CFR), Department of Electronics and Information Technology, Government of India, Chennai.He is a Certified Reliability Engineer (CRE) by American Society for Quality (ASQ, USA). He is also a certified Information Security Management System (ISMS 27001) Auditor from IRCA, U.K., and a certified ISO 9000 system Auditor from BSI – QA, U.K. He has about 26 years of experience in the area of Reliability Prediction, GrowthTesting, Reliability Statistics, and Quality Assurance of Electronics and IT products. He is a lead faculty in the "Certified Reliability Professional" training program of Government of India. He has to his credit over 27 research papers in International and National Journals/ Conferences and Magazines. He has been trained in Quality and Reliability in U.K., France, USA and Germany.*

He was the project leader for Reliability studies of various subsystems of PSLV/GSLV rocket systems for ISRO, Light Combat Aircraft and Advanced Light Helicopters for DRDO Labs, Verification and Validation of Anti Collision Device (ACD), Axle counter systems for Railways and various other projects from automobile sector. He is also the project leader for implementing "Process Reliability Management" for Vizag Refinery of Hindustan Petroleum Corporation Ltd., Vizag. He was project leader for many HALT projects, HASS projects, Reliability Determination Testing projects and Accelerated Reliability Testing projects.

He holds a Bachelor's degree in Electronics and Communication Engineering, Master's degree, M.S. in Electronics Engineering, a post graduate Diploma in Business Administration and obtained his doctoral degree in Embedded Systems Reliability.

Life Cycle Reliability and Safety Engineering
Vol.5 Issue 2 (2016) 01-07

Orbital TIG Welding Process Parameter's Effect on Porosity in Design of Experiment for Satellite Application

M Karthikeyan*[1], VNA Naikan[2], R Narayan[1], D P Sudhakar[1]

[1]*Liquid Propulsion System Centre (LPSC), Indian Space Research Organisation, Bangalore*
[2]*Reliability Engineering Centre (REC), Indian Institute of Technology, Kharagpur*
*Email: [1]*kavimukthe@gmail.com*

Abstract

This paper highlights the effect of parameters of Orbital Tungsten Inert Gas (OTIG) weldments on porosity employing Design of Experiment (DOE) using Taguchi method for stainless steel tubes used in propulsion feed system in satellites. This proposed methodology identifies the optimum parameters for welding and brings out the significance of the individual parameter on porosity and combination of any of the two parameters (interaction effect) using Taguchi method by linear model analysis of Porosity verses input parameters. This proposed method is applied for welding of stainless steel tubes of 6mm diameter and 0.7 mm thickness for propellant feed system of satellites. Further these are tested by different methods to evaluate the strength required for intended application. Detailed experiments were carried out using L27 Taguchi method and optimum parameters are arrived. Further the effect of porosity is studied. This ensures sound and reliable weld joint. The optimum levels of these parameters thus developed are being followed and no need for any rework is reported thereafter. By varying the input parameters (current, RPM, gap between electrode and the job), the weld penetration level or weld quality has been studied in several 6mm diameter tube specimens. The Factorial Factor design is followed for minimum of 27 (3^3=3x3=27) samples for this experiment. By varying the input parameters, the significance were studied and discussed in the test results. By further fine tuning the experiment, the optimized values are validated by studying the effect of porosity on individual parameters and their combination effect. From the experiment it was found that Current has the most significant effect on the porosity. It is also found that the effects of rest of the parameters are negligible. The weld specimen quality was verified in accordance with the user's quality standards and found satisfactory. The experimental findings are thus validated. The proposed approach provides an easy to develop and easy to use method that assures the best combination of parameters required for Orbital TIG welding which yield strong and defect free weld joint for Satellite application.

Keywords—OTIG; weld parameters; propulsion; satellite integration; porosity; optimal current.

1. Introduction

The propulsion system provides the reaction control capability for attitude control and orbit positioning in Polar & Geosynchronous orbits. The propulsion configuration consists of many components and includes 6mm & 10mm outer diameter plumb lines (Propellant feed lines) end connection with thickness of 0.7mm requiring Orbital TIG welding during final integration of Satellites. The factors affecting the weld joints are precise control of weld current, voltage input, gap between work pieces (plumb lines with propulsion components), gap between electrode and work pieces, selection of electrode geometry, bandwidth, electrode travel speed (RPM), flow rate of shielding gas used etc. The variation of any of these parameters will certainly affect quality of weld in the propulsion system resulting in weld defects such as undercut, lack of penetration, non-uniformity, cracks, excessive weld bead width, excessive weld-puddle overlap etc. Hence it becomes necessary to optimize the parameters. Here control of weld current, RPM and gap between electrode and tube are taken as parameters for study purpose. The effect of porosity study was done to evaluate the impact of individual parameter and combination of parameters on the quality and reliability of weldments for Spacecraft Propulsion system. This analysis involves selection of different matrices as shown in the Table. IV to

determine the quality of each weld joint minimizing the porosity. Further to this analysis, optimized values/ measures were suggested to avoid porosity. Therefore the analysis has been performed based on parameters given in the table during integration phase of propulsion system to achieve defect free welding and ensure high reliability.

The propulsion system is configured as shown in the Fig. 1, There are about 350 numbers of Orbital TIG weld joints to interconnect propulsion components using 6mm and 10 mm plumb lines.

As the feed lines carry the propellants to the propulsive device, any leak in the welds will lead to disaster. In view of this, it is essential that all the joints in the propellant feed lines need to be totally leak proof. In order to ensure this, the effects of porosity on the weldments caused by the parameters are discussed in this paper

2. Literature Survey

Orbital TIG welding for feed lines of a propulsion system is a specialized application and hence not many literatures are available in public domain. However, the related welding investigations carried out by others are given here. Mike Sarafin [1] stressed the importance of high quality, integral weldments for space applications and outlined the merits of orbital welding towards this. Andrew and Franscois [2] covered the details of MMH/NTO bipropellant propulsion system involving propellant feed system that helps for transfer orbit manoeuvres and station keeping operations. Peter [3], highlighted the importance of leak proof propellant storage and feed systems and outlined the failure of a communication satellite launched by Ariane 5 rocket due to leak in feed system. A small leak of propellant can lead to a failure of a big mission with huge cost and enormous efforts. Claude [4] has enlisted spacecraft failures and the reasons there of since 1957. Shih Chang [5] clearly enumerated the huge losses (in millions of dollars) due to launch failures and analyzing the failure between 1957 and 1999 indicated that out of 4378 launches, 390 failed and major causes pointed to propulsion system failure due to fuel leakage among other reasons. Prachya [6] studied the shielding gas effect on properties of HAZ and fusion zone on GTAW of Al - alloy AA5083 evaluating hardness. Pradeep and Sorte [7] have shown that the welding input parameters play a very significant role in determining the quality of a weld joint with minimum distortion. Kumar [8] studied TIG parameters and pitting corrosion of Al - alloys using ANOVA, regression analysis and mathematical models. Kumar and Sundarrajan [9] have presented the results of extensive research on improving the mechanical properties of AA 5456 aluminium alloy welds by pulsed TIG deploying Taguchi method, regression models and analysis of 'variance'. Sudhakar [10] analyzed the brazing parameters for joining stainless steels by Ni braze alloy for rocket chamber application by employing L9 Taguchi orthogonal array and AVOM and ANOVA. Jose [11] researched on these welding programs for orbital TIG welding i.e., pulsed current & increasing speed, constant current, pulsed current & decreasing speed and suggested that constant current provided better results based on mathematical tests.

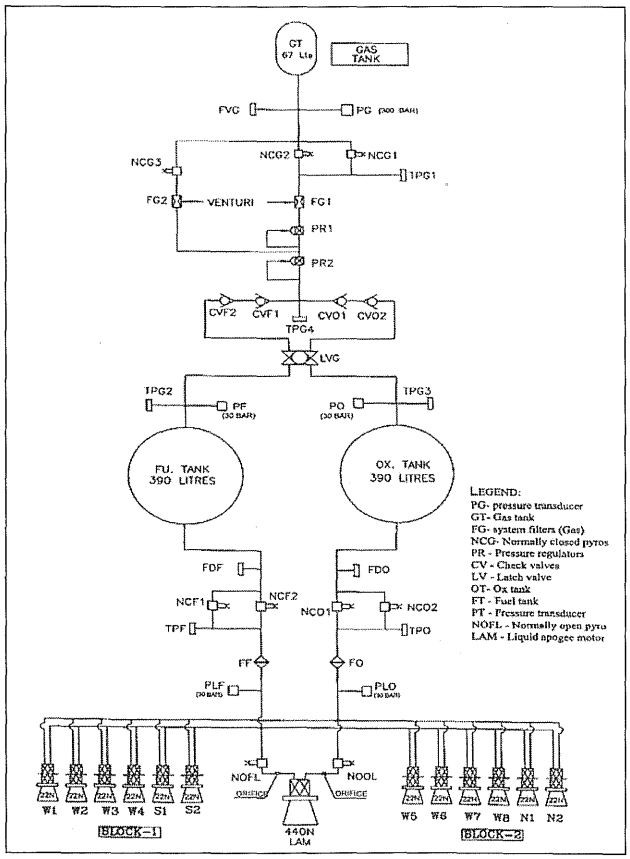

Fig. 1. Feed lines (propulsion schematic)

The literature that reported the effects of weld parameters on porosity for OTIG welding process is very minimal and almost nil for this kind of applications and hence it is felt essential to undertake this study which will provide more insight in this area.

3. Plan of Investigation

In this work, the OTIG welding process is analyzed by experimental methods. Good quality welding is influenced by several parameters (variables and constants) such as current, RPM, gap between electrode

and tubes, gap between tubes where they butt each other, thickness of the tube, purge/shield gas, electrode geometry, and voltage input etc. These are enumerated in the Table I. The cleanliness of tubes is another factor to be considered prior to welding as it influences the porosity. Similarly the shield gas used for the welding is ensured for negligible moisture content. This study is focused on only those parameters to minimize porosity to increase strength. The following steps are involved in carrying out this experiment.

Table I. Variables and Constants (Parameters)

Parameters (their units)	Range	Type V/C*
Current (Amps)	17.8 to 18.9	V
RPM (Nos)	9 to 10.5	V
Gap: Electrode & Tubes (mm)	0.7 to 0.9	V
Gap between Tubes (mm)	0.05 to 0.5	V
Thickness of Tubes (mm)	0.7	C
Purge Gas flow (Psi)	3 to 4	V
Electrode Geometry (mm)	Sharp/ Wider	V
Voltage input (Volt)	240	C

** V-Variable, C-Constant*

A. Identification of Parameters and Range

The ranges in which the variable and constant parameters are being used for performing the welding experiments are given in Table II. Only three parameters that have direct significant impact in the soundness of weld joints such as current, RPM and gap between electrode and tubes are chosen for this experiment to evaluate the extent of the porosity.

Table II. Identification of Process Parameters

Factors	Low (L)	Medium (M)	High (H)
Current (C) (Amps)	17.8 (C1)	18.35(C2)	18.9(C3)
RPM(R) (Nos.)	9.5(R1)	10(R2)	10.5(R3)
Gap(G) (mm)	0.7(G1)	0.8(G2)	0.9(G3)

B. Material Properties

Propulsion system employs both stainless steel tubes and titanium tubes. For this experiment stainless steel 304L tube is used. The parent metal, its Chemical Composition and Mechanical properties are furnished in Table III.

Table III. Chemical and Mechanical Properties of SS 304L

Chemical Composition of SS 304L: Percent by Weight			
C	0.03	S	0.03
Cr	18-20	Si	0.75
Ni	8-12	Al	0.1
Mn	2	Fe	Balance
P	0.045		
Mechanical Properties of SS 304L			
Tensile strength Ultimate	590 MPa	Melting Point	1399 - 1454°C
Yield Strength	250 MPa	Percent Elongation	35-50%
Comp. Strength	250 MPa	Hardness	80(Rc)
Density	7890 kg/m^3	Young Modulus	200 GPa
Poisson ratio	0.29		

C. Design of Experiments (DOE)

Taguchi methods are statistical methods developed to improve the quality of manufactured goods and more recently applied to other domains. The different reasons that cause variation in design parameters and in the manufacturing process are termed as noises. The optimum and most efficient way to solve these problems of variation is to make the design & process insensitive to the effect of noises which are the causes of variation. This underlying principle of robust design is the back bone of Taguchi analysis. It is a scientifically disciplined mechanism for evaluating and implementing improvements in a process with parametric optimization for the objective function, minimizing the effects of undesirable noises. Analysis of variance (ANOVA) is similar to regression in that it is used to investigate and model the relationship between a response variable and one or more independent variables. In this study general linear model is used to determine the influence of welding speed, current and gas flow rate on ultimate tensile strength and porosity. After conducting the experiments, the data taken are analyzed to determine the effects of various parameters. The experiments were in the form of L27 (3^3) orthogonal array as shown in Table IV. This array has three columns for process parameters and twenty seven rows of the

combination of parameters used for conducting the experiments and study three levels of parameters.

4. Experimentation

OTIG welding experiments were initially carried out on specimens and then on tubes of diameter 6mm and thickness 0.7mm as per the L27 matrix given in Table IV. The welded specimens were tensile tested after radiography and bend tested subsequently. The porosity levels were studied.

Fig. 2 shows the welding experiment set up. After getting satisfied with the results of specimen, trials

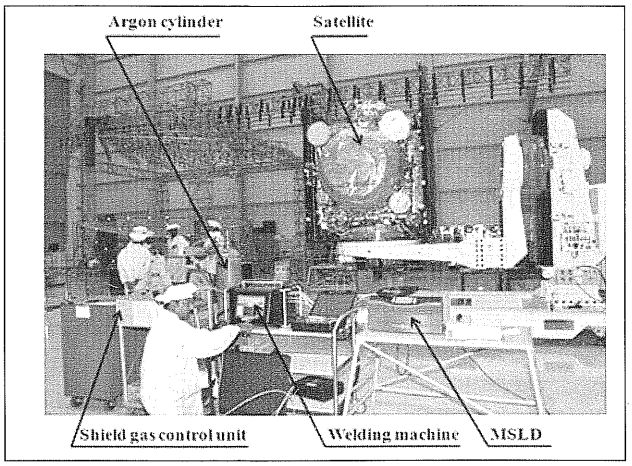

Fig. 2. Experimental set up for OTIG welding

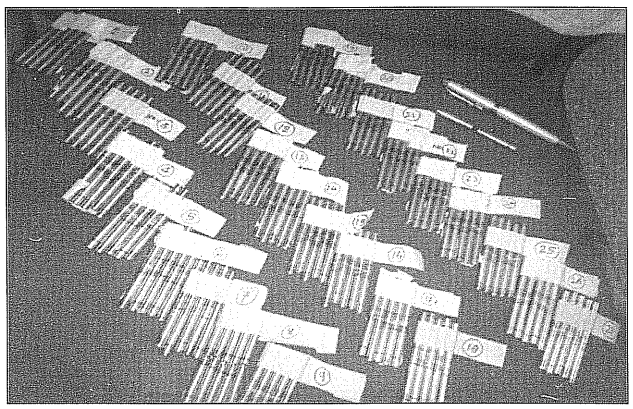

Fig. 3. L-27 Matrix welded tubes

were made on 6mm tube used for propellant feed lines in experimental set up as shown on Fig.2. As explained in section III *A*, the three important welding parameters namely Current, RPM and the distance between the electrode and the tube were experimented at three levels i.e. low, medium, high of each. Totally 27 experiments were conducted as per L27 array of experiments. The welded tube specimens are shown in Fig. 3, as per L27 design.

Optimization was done to find optimum welding conditions to maximize tensile strength and minimize porosity of welded specimen.. The tensile tests were carried out according to the ASTM standards. Twenty seven specimens were as input matrix of Taguchi design and values obtained are given in Table IV. The welded tubes as seen in X-ray film is given in Fig. 4. The allowable porosity level is 0.3 mm for satellite feed lines. The porosities seen in the X-ray

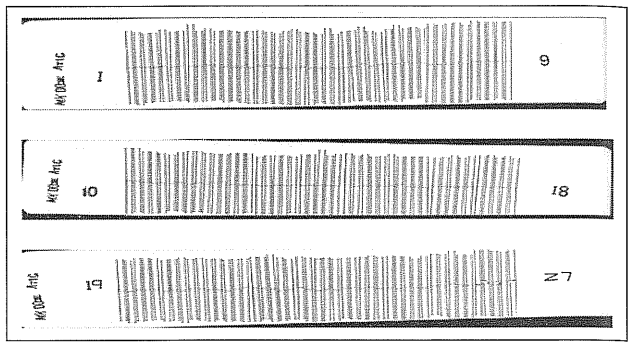

Fig. 4. Welded tubes in X-Ray film

Table IV. Experimental Layout using L27 Array and Responses

Sr. No.	C	R	G	C	R	G	P Trial -1	P Trial -2	UTS (N/ mm^2)
1	C1	R1	G1	17.8	9.5	0.7	0	0	407.10
2	C1	R1	G2	17.8	9.5	0.8	0	0	447.39
3	C1	R1	G3	17.8	9.5	0.9	0	0	470.47
4	C1	R2	G1	17.8	10	0.7	0	0	485.98
5	C1	R2	G2	17.8	10	0.8	0	0	501.01
6	C1	R2	G3	17.8	10	0.9	0	0	535.54
7	C1	R3	G1	17.8	10.5	0.7	0	0	541.16
8	C1	R3	G2	17.8	10.5	0.8	0	0	547.72
9	C1	R3	G3	17.8	10.5	0.9	0	0	551.45
10	C2	R1	G1	18.35	9.5	0.7	0	0	566.84
11	C2	R1	G2	18.35	9.5	0.8	0	0	562.70
12	C2	R1	G3	18.35	9.5	0.9	0	0	578.33
13	C2	R2	G1	18.35	10	0.7	0	0	585.55
14	C2	R2	G2	18.35	10	0.8	0	0	591.60
15	C2	R2	G3	18.35	10	0.9	0	0	582.78
16	C2	R3	G1	18.35	10.5	0.7	0	0	563.31
17	C2	R3	G2	18.35	10.5	0.8	0	0	557.92
18	C2	R3	G3	18.35	10.5	0.9	0	0	556.03
19	C3	R1	G1	18.9	9.5	0.7	0.4	0.8	547.96
20	C3	R1	G2	18.9	9.5	0.8	0.6	0.8	546.41
21	C3	R1	G3	18.9	9.5	0.9	0.4	0.6	539.40
22	C3	R2	G1	18.9	10	0.7	0.6	0.6	512.03
23	C3	R2	G2	18.9	10	0.8	0.6	0.6	499.16
24	C3	R2	G3	18.9	10	0.9	0.9	0.6	472.71
25	C3	R3	G1	18.9	10.5	0.7	0.9	0.9	460.77
26	C3	R3	G2	18.9	10.5	0.8	0.16	0.15	436.17
27	C3	R3	G3	18.9	10.5	0.9	3	3	337.25

C-Current, R-rpm, G-gap, P-porosity,

varies from 0.2mm to 0.4mm. Three numbers of 0.2mm porosity is given in the Table IV as 0.6mm (3x0.2=0.6) and similarly three numbers of 0.3mm porosity is given in the Table IV as 0.9mm(3x0.3=0.9). The hole formation due to 27th row matrix is 3mm.

5. Analysis of Data and Recording the Responses (Porosity Trial 1 &2)

The common one among the defects encountered in the orbital TIG welding is Porosity. Porosity is a collective name describing cavities or pores caused by gas and non-metallic material entrapment in molten metal during solidification. There are many causes which include contamination, inadequate shielding, unstable arc, too short an arc gap and poor welding technique in general.

The higher-the-better performance characteristic is expressed

$$S/NHB = -10 \log \{(1/y12+1/y22...1/yn2)/n\} \quad (1)$$

Where n is the number of repetition of output response in the same trial and y is the response. Table V shows the result of porosity Trial 1 & 2.

Table V. Results of Signal to Noise Ratio Analysis

C	R	G	P Trial-1	P Trial-2
17.8	9.5	0.7	0	0
17.8	9.5	0.8	0	0
17.8	9.5	0.9	0	0
17.8	10	0.7	0	0
17.8	10	0.8	0	0
17.8	10	0.9	0	0
17.8	10.5	0.7	0	0
17.8	10.5	0.8	0	0
17.8	10.5	0.9	0	0
18.35	9.5	0.7	0	0
18.35	9.5	0.8	0	0
18.35	9.5	0.9	0	0
18.35	10	0.7	0	0
18.35	10	0.8	0	0
18.35	10	0.9	0	0
18.35	10.5	0.7	0	0
18.35	10.5	0.8	0	0
18.35	10.5	0.9	0	0
18.9	9.5	0.7	0.4	0.8
18.9	9.5	0.8	0.6	0.8
18.9	9.5	0.9	0.4	0.6
18.9	10	0.7	0.6	0.6
18.9	10	0.8	0.6	0.6
18.9	10	0.9	0.9	0.6
18.9	10.5	0.7	0.9	0.9
18.9	10.5	0.8	0.16	0.15
18.9	10.5	0.9	3	3

The above Table V. shows the result obtained from the orthogonal array and porosity. Here there is a need to increase the strength of the tube, hence higher-the-better is selected and the main effects for the porosities are plotted.

6. Experimental Results and Discussion

A. Effect of Parameter Analysis

Analysis of Variance (ANOVA) is used to investigate and model the relationship between a response variable (Porosity) and one or more independent variables. In this study, Taguchi notation tells the number of runs, factors, and levels for each factor in the design. In this example, the notation L27 (3^3) means a Taguchi orthogonal array with 3 factors with 3 levels each. In this experiment the porosity is the indirect measure of strength of the weldment.

A dynamic response experiment, in which the goal is to optimize the relationship between the input and the output of the system, includes a signal factor. Taguchi linear model is used to study the influence of welding current, RPM, gap between tube and electrode on Porosity. In this experiment, the influence of individual parameter and combination of parameters are also studied. The following are the effects or results of parameters.

Taguchi experiment was carried with linear model analysis with current, RPM and gap between electrode and tube as source variables and Porosity as response variable.

General Linear Model: Porosity1 versus Current, RPM, Gap

Factor	Type	Levels Values
Current	fixed	3 17.80, 18.35, 18.90
RPM	fixed	3 9.5, 10.0, 10.5
Gap	fixed	3 0.7, 0.8, 0.9

Table VI. Variance for Porosity 1, using Adjusted SS for Tests

Source	DF	Seq SS	Adj SS	Adj MS	F	P
Current	2	4.2336	4.2336	2.1168	9.09	0.009
RPM	2	0.4225	0.4225	0.2112	0.91	0.442
Gap	2	0.5443	0.5443	0.2721	1.17	0.359
Current* RPM	4	0.8450	0.8450	0.2112	0.91	0.504
Current* Gap	4	1.0885	1.0885	0.2721	1.17	0.393
RPM* Gap	4	0.9316	0.9316	0.2329	1.00	0.461
Error	8	1.8633	1.8633	0.2329		
Total	26	9.9288				

S = 0.482609 R-Sq = 81.23% R-Sq(adj) = 39.01%

Table VII. Unusual Observations for Porosity 1

Obs	Porosity1	Fit	SE Fit	Residual	St Resid
26	0.16000	0.69778	0.40485	-0.53778	-2.05 R
27	3.00000	2.29778	0.40485	0.70222	2.67 R

R denotes an observation with a large standardized residual.

General Linear Model: Porosity2 versus Current, RPM, Gap

Factor	Type	Levels Values
Current	fixed	3 17.80, 18.35, 18.90
RPM	fixed	3 9.5, 10.0, 10.5
Gap	fixed	3 0.7, 0.8, 0.9

Table VIII. Variance for Porosity 2, using Adjusted SS for Tests

Source	DF	Seq SS	Adj SS	Adj MS	F	P
Current	2	4.8002	4.8002	2.4001	9.15	0.009
RPM	2	0.3202	0.3202	0.1601	0.61	0.567
Gap	2	0.4146	0.4146	0.2073	0.79	0.486
Current* RPM	4	0.6404	0.6404	0.1601	0.61	0.667
Current* Gap	4	0.8293	0.8293	0.2073	0.79	0.563
RPM* Gap	4	1.0493	1.0493	0.2623	1.00	0.461
Error	8	2.0985	2.0985	0.2623		
Total	26	10.1524				

S = 0.512167 R-Sq = 79.33% R-Sq(adj) = 32.82%

Table IX. Unusual Observations for Porosity2

Obs	Porosity 2	Fit	SE Fit	Residual	St Resid
27	3.00000	2.23704	0.42964	0.76296	2.74 R

R denotes an observation with a large standardized residual.

The analysis shows Current is the most influencing parameter having rank 1, then the RPM stands second followed by the Gap between tube and electrode in the third place.

For the linear models (Trial 1&2), Current (p= 0.009 & 0.009) are significant at the 0.05 α-level. The remaining factor gap is not significant to the response.

If combination is considered for the porosity effect, current* RPM (p=0.504 & 0.667), current *gap (p=0.393 & 0.563) and RPM*gap (p=0.461 & 0.461) are not significant at the 0.05 α-level to the response.

R-Sq = 81.23% and R-Sq = 79.33% of Trial 1 &2 show that the process desired signal is more

Factors Current, RPM and gap between tube and electrode could explain the variability of response of UTS with 79.33%

By this analysis, the effect or significance and rank of individual parameters were obtained from the Linear Model Analysis of Porosities. In addition, the individual parameters contribution is also obtained from the Linear Model Analysis.

In the experiment, pin hole or burn through is observed due to high current. Due to that, the tensile strength obtained is the lowest among all values. This also apparently appeared in the anlysis as Unusual Observations for both the trials as 27th element.R denotes an observation with a large standardized residual. In Response Table for porosity, higher is better was chosen as higher the ultimate strength, it is always better.

B. Main and Interaction Effects

The main and the interaction effects on SN ratio are shown in the Fig. 5 and 6 respectively. Fig. 5 clearly shows that the mean of SN ratio increases with increase of current till 18.35Amps and decreases with increase of current further. The mean of SN ratio also increases with increase of RPM till 10 and decreases with increase of RPM further. However, this effect is not appreciable when compared to that with respect to the variation in the current. The mean of SN ratio does not significantly change with

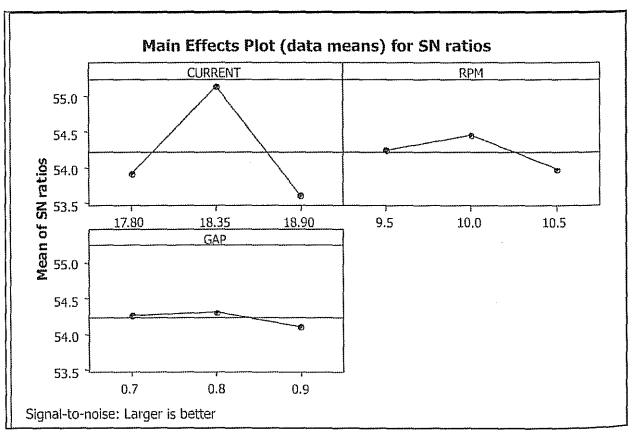

Fig. 5. Main Effect Plot for SN ratio

increase or decrease of the gap.Similar observations are seen for mean also in the main effect plot (Fig. 6).

7. Conclusions

This paper has presented the optimization

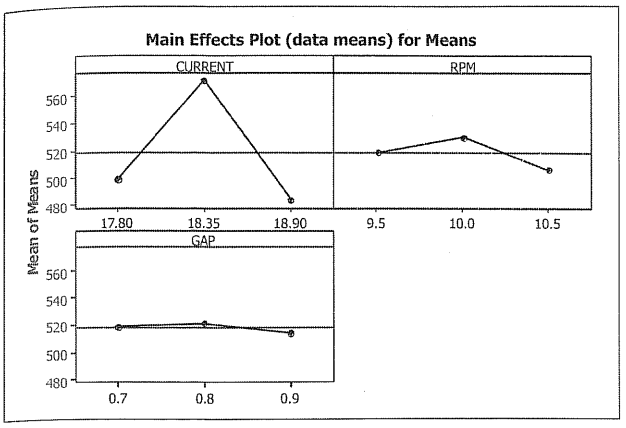

Fig. 6. Main Effect Plot for Means

of process parameters of OTIG welding of 6mm propellant feed tubes made of 304L Stainless Steel material for satellite system using statistical optimization techniques. Design of experiments as per Taguchi's L27 array was used for the study.

Taguchi linear model analysis of Signal to Noise (SN) ratio and means versus input parameters were carried out. Analysis of variance, interaction effects and residual plots were also made. Based on experimental results and confirmation tests, the following conclusions can be drawn.

- The optimum values obtained from the selected factors for welding of 6mm SS304L tube are Current 18.5 A, RPM 10 and Gap between tube and electrode 0.8mm.
- The most important parameter affecting the responses have been identified as Current and this is followed by the RPM. Therefore, keeping good control over the weld current is the key action which decides the weld strength and its quality.
- Validation of weld strength is determined by tensile test. Also it was found that there is good improvement in tensile strength values after optimizing the parameters. Hence a good quality weld is obtained from optimized current, RPM and gap chosen in the experiment.
- By this study, the optimized process parameters would definitely improve the reliability of propellant feed system for satellite propulsion which is highly essential for the successful space missions.

Acknowledgment

Authors wish to thank Shri S. Ravi, Shri V.N. Misale, Shri D. Saravanakumar and Dr. Heeralal Gargama for their useful contributions in this work. Authors wish to express their gratitude to Shri G. Narayanan, Deputy Director, SRQA, Shri.S. Somanath, Director LPSC and ASC Committee for their constant encouragements and kind permission to submit this paper in any technical journal.

References

1. Mike Serafin, "Orbital welding for space program applications: Producing welds that withstand the rigors of deep space," TPJ - The Tube & Pipe Journal. Cape Canaveral Air Force Station. http://www.thefabricator.com/article/tubepipefabrication/orbital-welding-for-space-program-applications--producing-welds-that-withstand-the-rigors-of-deep-space, 2001.
2. D. Andrew, and C. François, "Development Testing Of A New Bipropellant Propulsion System For The Gmp-T Spacecraft, European Space Agency (ESA-ESTEC)," Keplerlaan 1, P.O. Box 299, 2200 AG Noordwijk, The Netherlands, 2009.
3. B. Peter, and de Selding, "Brand New Satellite (Eutelsat W3B) Declared Dead after Launch," Space News Staff Writer, October 29, 2010.
4. Claude Lafleur, Space craft (known) failures, space craft encyclopedia. http://claudelafleur.qc.ca/Spacecrafts-index.html.
5. I. Shih Chang, "Space Launch Vehicle Reliability," The Aerospace Corporation Magazine of Advance in Aerospace Technology, http://www.aero.org/publications/crosslink/ winter2001/03.html, 2001.
6. Prachya Peasura, and Anucha Watanapa, "Influence of Shielding Gas on Aluminum Alloy 5083 in Gas Tungsten Arc Welding," International Workshop on Information and Electronics Engineering (IWIEE), Vol.29, pp. 2465 – 2469, 2012.
7. Pradeep Deshmukh, and M.B. Sorte, "Optimization of Welding Parameters Using Taguchi Method for Submerged Arc Welding On Spiral Pipes," International Journal of Recent Technology and Engineering (IJRTE), ISSN: 2277-3878, Vol. 2, Issue 5, pp. 50 – 54, 2013.
8. T. Senthil Kumar, V. Balasubramanian, and M.Y.Sanavullah, "Influences of Pulsed Current Tungsten Inert Gas Welding Parameters on the Tensile Properties of AA 6061 Aluminium Alloy," Materials and Design 28 (2007) 2080–2092 pp. 2080 – 2092, 2007.
9. Kumar, A. and Sundarrajan, S.(2009), Optimization of Pulsed TIG Welding Process Parameters on Mechanical Properties of AA 5456 Aluminum Alloy Weldments, Materials and Design 30 (2009), pp.1288–1297.
10. D.P. Sudhakar, M. Rajmohan, K. Jha Abhay, and A.E. Muthunayagam, "Optimisation of vacuum brazing conditions for joining Stainless Steel 321 sheets by Nickel based braze foil for regenerative rocket nozzle applications by Taguchi Method," Journal of Aerospace sciences and technologies, vol.63, No.3,pp 230-236, 2011.
11. A. Jose, Orlowski de Garcia, Nilton Souza Dias, Gérson Luiz de Lima, D. Wilson, Bocallão Pereira, and Nívio Fernandes Nogueira, " Advances of Orbital Gas Tungsten Arc Welding For Brazilian Space Applications," Experimental Setup, doi:10.5028/jatm.2010.02026610, Vol. 2, No.2, pp. 203 – 210, 2010.

Life Cycle Reliability and Safety Engineering
Vol.5 Issue 2 (2016) 08-11

Extreme Value Analysis of Rainfall Data for Kalpakkam

Pramod Kumar Sharma, A. John Arul, M. Ramkrishnan, V Bhuvana
Reactor Shielding and Data Division , Indira Gandhi Centre for Atomic Research, Kalpakkam, India
pramodks@igcar.gov.in

Abstract

Flood hazard evaluation is an important safety study for a Nuclear Power Plant. In the present study flood hazard at PFBR site due to rainfall is evaluated. Hazard estimation is a statistical procedure by which rainfall intensity versus occurrence frequency is estimated from historical records of rainfall data and extrapolated with asymptotic extreme value distribution. Rainfall data needed for flood hazard assessment is daily annual maximum rainfall (24 hrs data). The observed data points have been fitted using Gumbel, power law, and exponential distribution and return period has been estimated. The predicted 100 yrs return period rainfall for Kalpakkam ranges from 240mm to 365 mm in a day and 1000 yrs return period rainfall ranges from 320mm to 790 mm in a day. To study the stationarity of rainfall data a moving window estimate of the parameters (exponential distribution) have also been performed.

Keywords: Rainfall, Flood Hazard, Gumbel distribution, Power Law, Exponential distribution, Generalized Extreme Value distribution.

1.0 Introduction

Flooding due to intense rainfall is one of the external events to be considered for a nuclear power plant safety analysis [1]. The presence of water in many areas of the plant may be a reason for common cause failure for safety related systems, such as the emergency power supply systems or the electric switchyard, with the associated possibility of losing the external connection to the electrical power grid, the decay heat removal system and other vital systems. Considerable damage can also be caused to safety related structures, systems and components by the infiltration of water into internal areas of the plant, induced by high flood levels. Water pressure on walls and foundations may challenge their structural capacity. Deficiencies in the site drainage systems and non-waterproof structures may also contribute to flooding on the site. This has happened many times in the past, with consequent large-scale damage documented, and the possibility should be considered in the hazard evaluation and in the design of measures for site protection [1]. Flood level in an area of the site is determined by three factor namely (i) rainfall intensity, (ii) effective catchment area and (iii) effective drainage capacity. Meteorological parameters like rainfall follow a seasonal cycle and the continuous survey of any meteorological parameter reveals annual extreme values. Projection of extreme values of environmental parameters likely to be encountered in the future using historically observed data is normally handled by extreme value statistical methods. Confidence levels of the statistically derived value depend on the size of the data as well as the data scatter with respect to fitted probability distribution function. Statistically, one can also find out the probability of non-exceedence of the value in terms of a mean recurrence interval (MRI).

2.0 Methodology

Rainfall data forms an important input to estimate maximum water level at the proposed site. Rainfall intensity (annual maximum) such as hourly rainfall rates (mm/h) to rainfall rate over longer intervals of few days are needed for flooding analysis. The first type of data are used for designing the storm water drainage around the site while the other data in more detail are needed for generating design basis flood water level at inland sites which are often situated near a river course or dam. Although continuous recording rain gauge is preferred, in cases where the continuous measurement of rainfall data is not available, measurements carried out over discrete time intervals (i.e. 1 hour etc.) is made use of to arrive at running average data for desired duration(e.g. 24 hours, if the point of interest is daily rainfall). An adjustment factor, which depends on the interval between successive measurements, will have to be applied to the observed sequential data set to arrive at the 24 hour running average rainfall data [2]. In many cases, due to non availability of measured extreme values of 1 hr data, this data is approximated with from 24hr data with

the help of empirical equations. For selection of the appropriate distribution, the measured parameters (i.e., extreme values of meteorological parameter like rainfall) are plotted on a plotting paper. In the analysis of extreme values three types of asymptotic distribution are used. These distributions are known as Type I (Gumbel), Type II (Frechet) and Type III (Weibull) distribution [3]. The Gumbel distribution, also known as the *Extreme Value Type I* distribution, is unbounded (defined on the entire real axis), and has the cumulative density function

$$F(x) = exp\{-exp(-z)\},\ x \sim R; \quad (1)$$

Where $z=(x-\mu)/\sigma$, μ is the location parameter, and σ is the distribution scale $(\sigma>0)$. The cumulative probability can also be written as (by taking log two times)

$$x=\mu-\sigma ln[\{-ln F(x)\}] \quad (2)$$

Plotting x against F(x) gives a straight line. This property enables a visual check to be made of the extent to which a data set fits the Gumbel distribution.

Rainfall frequency is often estimated by power law fit and exponential distribution.

The cumulative distribution function of power law fit is

$$F(x) = ax^b, \quad x \sim R; \quad (3)$$

And the cumulative distribution function of Exponential fit is

$$F(x) = ae^{bx}, \quad x \sim R; \quad (4)$$

Plotting ln(x) against ln(F(x)) gives a straight line. This property enables a visual check to be made of the extent to which a data set fits the power law distribution.

Plotting x against ln(F(x)) gives a straight line. This property enables a visual check to be made of the extent to which a data set fits the exponential distribution.

The data set has also been plotted with Generalized Extreme value distribution.

3.0 Data Collection and Analysis

Rainfall data is gridded rainfall data obtained from IMD Pune for a period of 1901-2004AD [4]. The gridded rainfall data has been collected over 1°x1° longitude latitude high resolution daily rainfall data (24hrs) for the Indian Region. This corresponds to 111 km x111 km at equator. Rainfall data is arranged in 35x33 grid points for Indian region. This represents a rectangular box in which city is located and rainfall data over various grids have been recorded. Kalpakkam (12.56N, 80.18E) and Chennai (13.08N, 80.27E) fall within same grid as far as recording of rainfall is concerned. Fig. 1 represents a grid in which Chennai (*) and Kalpakkam (+) is represented. The total number of rainfall station within this grid (Kalpakkam) is 15. From data, it is not clear that rainfall data used in the analysis is average over these rainfall station or maximum observed over a station. It is also not clear that which station in nearest to Kalpakkam. A FORTRAN program has been written to retrieve data for a particular grid. The data extracted is maximum rainfall in a single day (24hrs) in a whole year. For 104 years a data set has been prepared, which is maximum daily rainfall for each year.

This data points have been fit using Gumbel distribution and return period has been estimated. The

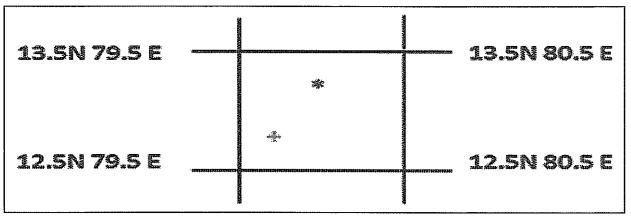

Fig.1: Kalpakkam(+) and Chennai(*) Latitude Longitude representation

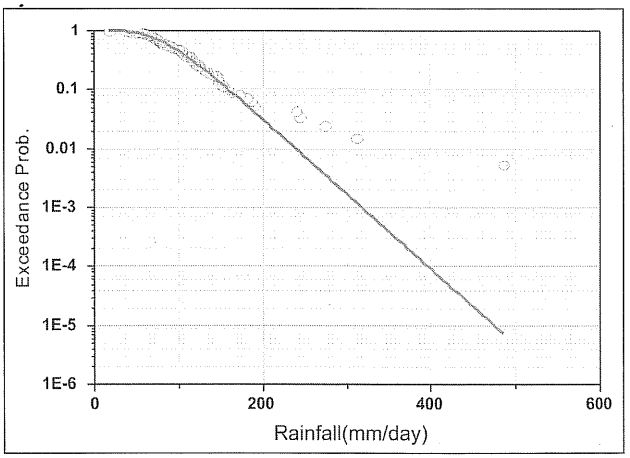

Fig.2: Observed Annual Maximum Rainfall in a Day for Kalpakkam vs. Log exceedance Probability

Gringorten plotting position [5] has been used for the analysis. As per Ref. [3], correction factor 1.13 has been used. The parameters for Gumbel fit has been shown in Table 1.The frequency of exceedance for observed and predicted by the Gumbel fit for various rainfall

levels are shown in Fig.2. The technique used for estimation of mean and standard deviation of Gumbel distribution is least squares fit.

The parameters for Gumbel fit has been shown in Table 1.

Table 1: Parameters of the Gumbel Fit to the Data

Parameter	Mean Values	Error	95% confidence Bounds
μ	82.52	0.2831	[83.09,81.95]
σ	34.13	0.43773	[34.98,33.26]

The 95% confidence bounds are estimated using the expression

Bounds = mean of the parameter ± (2*Error estimated for the parameter).

A fit to the Generalized Extreme value distribution yields a fit very close to Gumbel distribution as shown in Fig.3.

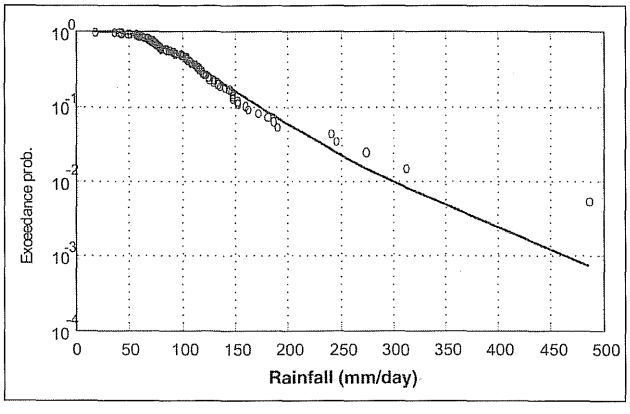

Fig.3: Observed Annual Maximum Rainfall in a Day for Kalpakkam vs. Log exceedance Probability (GEV)

The parameter for Generalized Extreme value distribution is given in Table2.

Table 2: Parameters of the Generalized Extreme Value Distribution to the Data

Parameter		
μ	Location parameter	81.83
σ	Scale parameter	35.01
κ	Shape parameter	0.123

As seen from the Fig.2, there are quite a few points which are deviating from the fitted line. Therefore power law and exponential fit are tried. For power law fit the data range considered is 100mm-500mm/day. Fig. 4 Represents power law fit for Log (Exccedance probability) vs Rainfall.

The entire set of Rainfall data for Kalapakkam has also been fit using exponential distribution and return period has been estimated. Fig. 5 Represents exponential fit for Log (Exccedance probability) vs Rainfall. The exponential fit gives higher estimate of rainfall in the region than Gumbel distribution but lower estimate than power law fit.

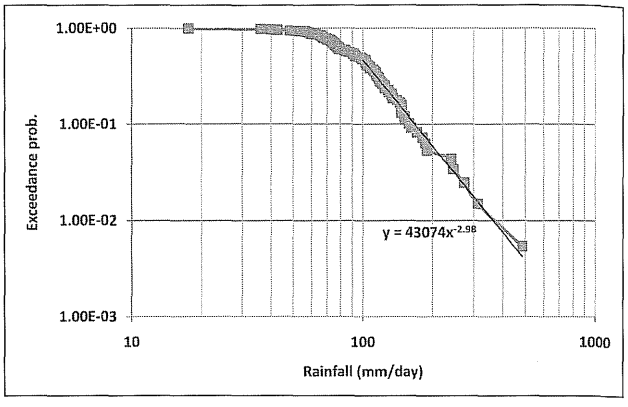

Fig. 4: Observed Annual Maximum Rainfall in a Day for Kalapakkam (Power Law fit)

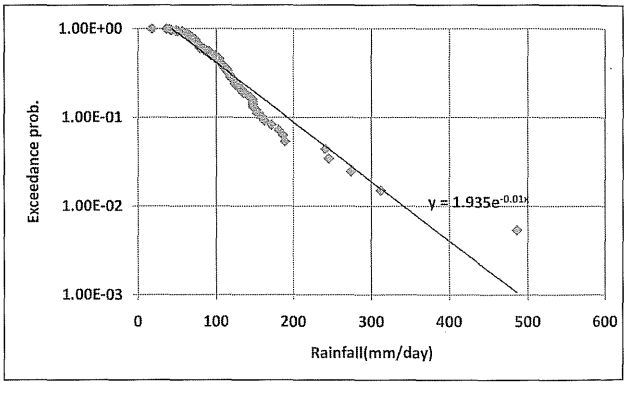

Fig. 5: Observed Annual Maximum Rainfall in a Day for Kalapakkam (Exponential fit)

4.0 Results and Insights

The predicted maximum rainfall for 100 years and 1000 years return period for Kalpakkam region by the Gumbel fit is shown in Table 3.

Table 3: Expected Rainfall

Return Period (Yrs)	Kalpakkam Rainfall (mm/day)	
	Mean	*95% UB*
100	240	245
1000	320	325
10000	400	410

The predicted maximum rainfall for 100 years and 1000 years return period for Kalpakkam region by power law fit and exponential fit is shown in Table 4.

Table 4: Expected Rainfall

Return period (Yrs)	Kalpakkam Rainfall (mm/day)		
	Gumbel fit	Power law	Exponential fit
100	240	364	344
1000	320	789	494
10000	400	1710	625

The goodness of fit for different model is shown in Table 5.

Table 5: Goodness of Fit for Sample data

Model	Reduced χ^2	Adj. R^2
Gumbel (0-500mm)	5.13×10^{-4}	0.994
Power Law (100-500mm)	1.02×10^{-4}	0.990
Exponential (0-500mm)	6.01×10^{-3}	0.929

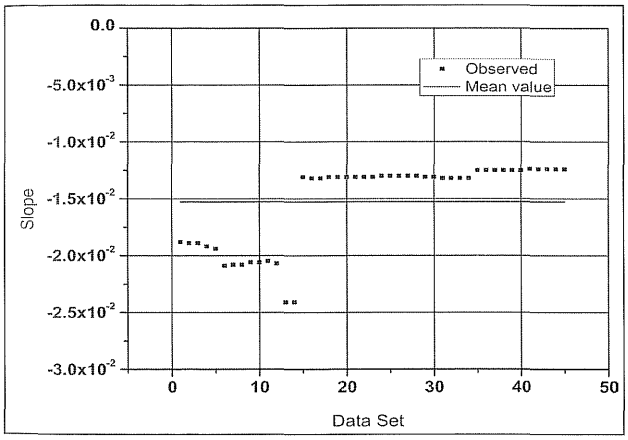

Fig. 6: Exponents variation with mean for Kalapakkam (Exponential fit)

To access the stationarity of the rainfall data, a moving window estimate of the exponent for the exponential fit is performed. The number of data points considered for each evaluation is 50 yrs and the evaluation is repeated ~ 50 times starting from year 1901-51. The obtained exponents are plotted in Fig 6. It is inferred from the plot that the exponent are almost constant from 1st set to 14th set and from 15th to 45th set. A small jump observed in the exponent after the 14th set is due to the occurrence of one extreme (1915-65) rainfall intensity of 486 mm in 1965.

It is to be noted that the maximum rainfall in a single day in Chennai is reported as 452 mm in 109 years (1901-08) [6]. The 1000 years return period predicted by Gumbel fit for Kalpakkam is 320 mm; however power law fit and exponential fit predicts 789 mm and 494 mm rainfall for 1000 years return period respectively.

5.0 Conclusions

Rainfall data needed for flood hazard analysis is hourly to daily maximum intensity. Historical rainfall data for about 100 yrs is obtained from IMD, Pune. Data for Kalpakkam region is extracted in the form of annual maximum of daily rainfall data. It is fitted with Gumbel distribution Power Law fit and Exponential fit to estimate the parameter to predict rainfall level corresponding to long term return period of 100 yrs, 1000 yrs and 10000 yrs. The predicted 100 yrs return period rainfall for Kalpakkam is 240mm-365 mm in a day and 1000 yrs return period rainfall is 320mm-790 mm in a day. The rainfall table shows that the different distribution gives different return periods for the same rainfall. Owing to the limited number of available data, the confidence intervals are very wide, and the predicted return periods are well inside the confidence interval. Hence the differences in return period are not significant, and one distribution is no better or worse than the other.

Acknowledgment

The authors are thankful to Dr. R. Venkatesan, RSD for his guidance and giving the data to the authors for carrying out this analysis.

References

1. International Atomic Energy Agency (2003). Flood Hazard for Nuclear Power Plants on Coastal and River Sites. Safety Guide, No. NS-G-3.5, Vienna.
2. Stedinger J.R., R.M. Vogel and E. Foufoula-Georgiou, 1993: Frequency analysis of extreme events. Chapter 18 (1-66) in: Handbook of Applied Hydrology; D.R. Maidment (Ed.) McGraw-Hill, NY.
3. Meteorological Events in Site Evaluation for Nuclear Power Plants. IAEA NS-G-3.4. 2003
4. High Resolution (1°x1°) Daily Gridded Rainfall Data for the Indian Region 1901-2004. National Climate Centre, Pune.
5. Onni S. Selaman,, Salim Said and F .J. Putuhena "Flood Frequency Analysis For Sarawak Using Weibull, Gringorten And L-Moments Formula" Journal - The Institution of Engineers, Malaysia (V ol. 68, No. 1, March 2007).
6. http://www.kea.metsite.com/ KEA weather station." Rainfall summary for Chennai city".

Life Cycle Reliability and Safety Engineering
Vol.5 Issue 2 (2016)12-14

Preliminary Tsunami Hazard Analysis For A Power Plant Site On East Coast Of India

M.Ramakrishnan[1], A. John Arul[2]

[1]*Probabilistic Safety Analysis Section, RSDD / RDG, Indira Gandhi Centre for Atomic Research Kalpakkam, India.*
[1]*Email: mramki@igcar.gov.in*

Abstract

The external flood PSA of PFBR is currently in progress. PFBR is located on the eastern coast of India which was severely affected by the 2004 tsunami. Hence the quantification of tsunami hazard is one of the important elements of external flood PSA of PFBR. The objective of the Tsunami hazard analysis is to quantify the wave run up heights on the shore for various return periods. A statistical analysis of Tsunami run up heights is reported for Kalpakkam in one of the earlier studies. This study under predicts the mean run up height as compared to the run up height observed during the 2004 event. The reason for this under prediction is the non-inclusion of local bathymetry. The present study improves the statistical analysis by including the local bathymetry into the model using work-energy theorem method.

Keywords– Tsunami hazard, bathymetry, runup height, return period, frequency of exceedence

1.0 Introduction

The Probabilistic Safety Analysis (PSA) of a nuclear power plant site includes both internal and external events. The procedure for carrying out PSA of external events is described in [1]. One of the important external risk contributors to a Nuclear Power Plant is flood. Flood PSA is carried out for NPPs based on national and international guidelines [2]. The flood PSA of Prototype Fast Breeder Reactor (PFBR) which is presently under construction at Kalpakkam is being carried out. This study includes three major activities. They are i) Flood Hazard Analysis ii) Flood Fragility Analysis and iii) Detailed system modelling and Development of accident sequences which leads to quantification of core damage frequency.

The flood hazard analysis for the site under consideration involves three major natural phenomena. They are i) Tsunami ii) Storm induced surges and iii) Local precipitation. Hazard curves are to be developed for each of these phenomena. In the present study tsunami hazard analysis is performed based on published literature. The tsunami hazard analysis can be divided into three parts. i) Characterization of Tsunami generating sources (like earthquake landslides, submarine volcano) ii) Wave propagation model and iii) Run-up and Wave Height model. The simulation of tsunami using elastodynamic equations for sea bed displacement and hydro dynamic equations for tsunami wave propagation and run-up is computationally intensive. The objective of the present study is to estimate preliminary run up height estimates for various return periods with a simple model for including local bathymetry.

2.0 Tsunami Hazarad Analysis For Kalpakkam Site

Tsunami Hazard Analysis for Kalpakkam is performed and reported [3]. In the reported study, a rectangular area between latitude 15°S and 15°N, and longitude 70°E and 12°E has been considered and data of earth quakes in this region have been compiled from the database of NEIC and NOAA. Earthquakes having magnitudes >5.0 are considered to have the potential to generate tsunamis. A relationship (1) between wave runup height(h), earthquake magnitude(M) and distance(D) from earthquake source is derived based on regression analysis of observed data.

$$h = C_1 \exp(C_2 M)(D+\varepsilon)^{-C_3} \quad (1)$$

c_1, c_2 and c_3 are the parameters which are determined by regression analysis. ε is the distance correction factor. The probability of earthquake occurrence in a time span of t years is assumed to follow a Poisson process. The probability of exceeding a certain wave

height is computed from this Poisson model and using (1). Two curves are reported in [3]. The first curve gives the tsunami wave run up height as a function of distance from source for the 26th December 2004 event. It is shown in fig.1.The second curve gives the tsunami wave run up height for different return periods. Following are the observations from the two curves reported in [3].

a) There is limiting value of tsunami run up height beyond which it is not increasing. But with the limited data on tsunami run up height, it is better to have some conservative estimate for tsunami run up height.

b) The predicted run up heights using (1) for the December 26, 2004 tsunami event is shown in fig.1. The predicted run up heights from (1) agrees well with the observed run up heights for large distances (distances more than 3000 Km). For Kalpakkam site, the under ocean faults are located at a distance of 1000-1500 Km. In this region, many observed run up heights are under predicted by (1). One of the reasons for this under prediction is the non-inclusion of bathymetry data specific to the site.

3.0 Improved Method For Tsunami Hazard Analysis

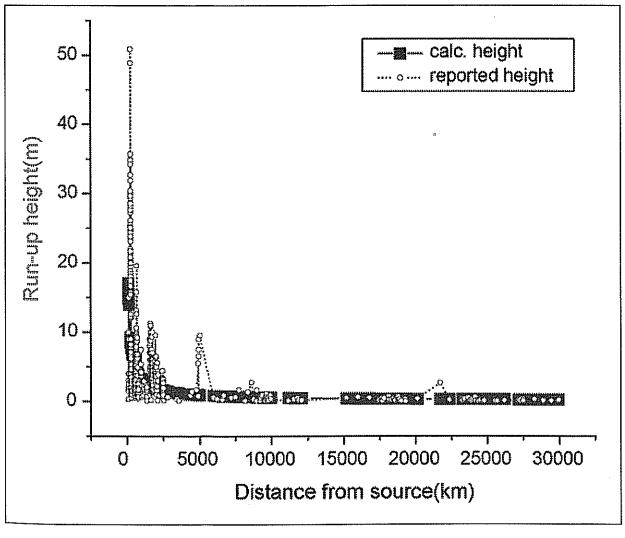

Fig.1. Variation of Tsunami Run up Height with Distance-Observed and Predicted values [3]

The prediction of tsunami run up heights in the previous section can be improved by including the local bathymetry for Kalpakkam. A simplified model to include local bathymetry is needed. The Work-energy theorem method is identified as a simple model to achieve this objective.

A. Work-Energy Theorem Method

The work-energy theorem method [4] attempts to derive the tsunami wave run up heights based on the principle of conservation of energy. The work-energy theorem (2) states that the sum of initial total mechanical energy (E_i) and the work done by the external forces (W_e) is equal to the final total mechanical energy (E_f). The mechanical energy can be potential energy or kinetic energy.

$$E_i + W_e = E_f \quad (2)$$

A tsunami wave approaching the coast contains both kinetic and potential energy. The external work done by wind (W_e in (2)) is considered to be negligible. As it advances to shallower waters its velocity decreases and height increases. The work is being done by the wave as it climbs the beach and the energy of the wave is gradually dissipated. Ultimately, the volume of water comes to a rest position. The work done reduces the kinetic energy from the wave. An expression is derived for tsunami wave run up height using this principle which is given by (3). This relationship tries to estimate the beach run up height from the tsunami wave height at zero metre depth and offshore angle.

$$H = (g/d)^{0.5}.H_0.t_c.\tan(\theta_b) \quad (3)$$

H is the beach run up height and H_0 is the wave height at zero metre depth. θ_b is the beach slope angle. g is acceleration due to gravity and d is the depth information used to calculate t_c. The depth used to calculate t_c in this study is 1m. t_c is the time tuning coefficient which is defined as the time taken by the wave to travel from 1m depth to 0m depth. The time tuning coefficient t_c follows an empirical relationship with offshore angle which is given by (4).

$$t_c = 0.6791[\tan(\theta_{off})]^{-1.0606} \quad (4)$$

θ_{off} is the off shore slope angle. Fig.2 gives the geometry of off shore slope, beach slope and wave height at mean sea level. The wave height at zero metre depth (H_0) is denoted by OZ in fig.2.

B. Bathymetry Data for Kalpakkam and Assumptions in this study

The off shore slope of Kalpakkam beach is measured at a distance of 125m from the coast line for four profiles [5]. The slope varies from 34° to 60° before the 2004 Tsunami event, and it is from 44° to 65° after the 2004 tsunami event. Broadly the slope

varies from 30° to 65°. The following assumptions are made in this study.

a) The beach is having a gentle gradient and the beach angle is equal to the off shore angle ($\theta_b=\theta_{off}$). Equation (3) can be used to calculate beach run up heights for plain beaches without any obstruction. Equation (3) gives the maximum vertical run up height. The run up heights predicted by (3) are conservative if obstructions like bunds, protection walls etc. are present in the beach.

b) It is further assumed that the run up height predicted by equation (1) is the wave height at zero metre depth for work-energy theorem method.

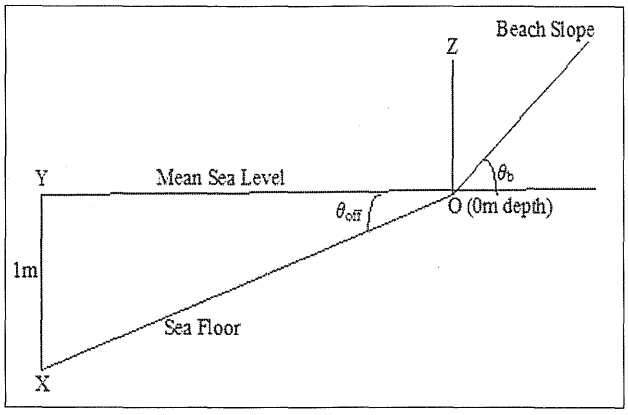

Fig.2: Geometry used in work energy theorem method

c) The beach slope varies from 30° to 65°. The beach slope of 30° is used in this analysis as it gives a conservative estimate of run up heights.

4.0 Results & Conclusion

The tsunami hazard curves generated for Kalpakkam site are given in fig.3. The hazard curve gives the frequency of exceedence as a function of tsunami run up height. The hazard curves reported in the earlier study and the curves obtained from the present study are shown in fig.3. The inclusion of bathymetry increases the tsunami wave run up height predictions. The mean and one sigma upper bound curves are given in Fig.3. During the 2004 Tsunami event, the maximum water level observed is ~4.7m above MSL.

The Tsunami wave run up height predicted by the earlier study and present study are compared

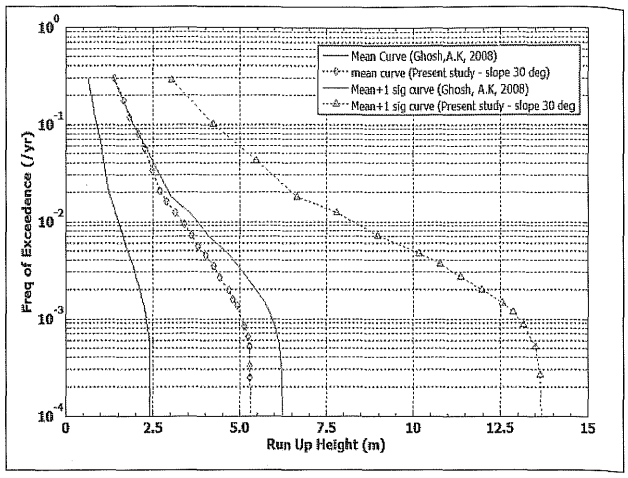

Fig.3: Tsunami Hazard Curves for Kalpakkam Site

in Table-1 for different return periods. The reported run up heights are with respect to Mean Sea Level (MSL).

Table-1: Tsunami Runup Height Comparison

Return Period (y)	Run Up Height - Earlier Study (m)		Run Up Height - Present Study (m)	
	Mean	*Upper Bound*	*Mean*	*Upper Bound*
100	**1.5**	**3.7**	**3.4**	**8.2**
1000	2.2	6.0	5.1	13.0
10000	2.4	6.2	5.3	13.6

Acknowledgment

The authors are thankful to Associate Director, CDG, Director RDG and Director, IGCAR for their support and encouragement in carrying out this study.

References

1. USNRC, PRA Procedures Guide, NUREG / CR-2300, Volume-II, 1983.
2. IAEA , Flood Hazard for Nuclear Power Plants on Coastal and River Sites. Safety Guide, No. NS-G-3.5, Vienna, 2003.
3. Ghosh, A.K, Assessment of earthquake-induced tsunami hazard at a power plant site, Nuclear Engineering and Design, 238, pp 1743-1749 2008.
4. Muraleedharan. G, Mourani Sinha, Rao A.D and Murty T.S., "Statistical Simulation of Boxing Day Tsunami of the Indian Ocean and a Predictive Equation for Beach Run up Heights Based on Work-Energy Theorem", Marine Geodesy,29, pp: 223-231, 2006.
5. Anandan. C and Sasidhar. P, "Assessment of the impact of the Tsunami of December 26,2004, on the near-shore bathymetry of the Kalpakkam Coast, East Coast of India", Science of Tsunami Hazards, Vol 27, no 4, pp: 26-35, 2008.

Life Cycle Reliability and Safety Engineering
Vol.5 Issue 2 (2016) 15-19

Physics of Failure Based Analysis of Aluminium Electrolytic Capacitor

Satya Ranjan Sahoo[1*], S.K. Behera[1], Sachin Kumar[2], P.V. Varde[2], G Ravi Kumar[3]
[1]*Department of Electronics and Instrumentation Engineering, NIT Rourkela, Odisha*
[2]*Research Reactor Services Division, Bhabha Atomic Research Centre, Mumbai*
[3]*Scientific Information and Resource Division, Bhabha Atomic Research Centre, Mumbai*
sahoosatyaranjan18@gmail.com

Abstract

Electrolytic capacitors are one of the important devices in various power electronic systems, such as motor drives, uninterruptible power supply, electric vehicles and dc power supply. Electrolytic capacitors are also the integral part of many other electronic devices. One of the primary function of electrolytic capacitors is the smoothing of voltage ripple and storing electrical energy. However, the electrolytic capacitor has the shortest lifespan of components in power electronics. Past experiences show that electrolytic capacitor tends to degrade and fail faster under high electrical or thermal stress conditions during operations. The primary failure mechanism of an electrolytic capacitor is the evaporation of the electrolyte due to electrical or thermal overstress. This leads to the drift in the values of two important parameters- capacitance and equivalent series resistance (ESR) of the electrolytic capacitor. An attempt has been made to age the electrolytic capacitor and validate the results. The overall goal is to derive the accurate degradation model of the electrolytic capacitor.

Keywords: Equivalent series resistance, thermal overstress, capacitance

1.0 Introduction

In the application of large aluminium electrolytic capacitors, the circuit designer faces the problem of obtaining the maximum possible ripple current in the smallest possible package with an acceptable capacitance and useful life. This life time is feasible in environment wherethe optimum temperature surrounding the capacitor is largely dependent onthesurrounding temperature, dissipation of power by the capacitor andsurroundingcomponents.If the ripple current is pushed too high to reduce the number of capacitors needed, then the rise of temperature due to the equivalent series resistance (ESR) is excessive [1].

If the capacitors are miniaturized, the smaller package size becomes a less efficient heat dissipater, and the ESR is alsoincreased. In either case, the higher temperatures generated internally to the capacitor lead to a shortening of the expected life. There are many approaches in solving this enigma. The usual approach is to specify a capacitor with a higher rated temperature such as 105°C. This approach is unavoidable when the core temperature cannot be reduced below 95°C.Anotherapproach is to lower the ambient air temperature. Specification of very low ESR reduces the heat load on the capacitor ,but the limits of low ESR technology are being pushed in many instances already. Circuit designers can also request capacitors with low internal thermal resistance to minimize the rise of the core temperature above the ambient temperature. In cases where efficient heat sinks are economical, the external thermal resistance of the capacitors can be improved. If space is available, the use of larger capacitor packages or Integral Heat Sinks can lower the external thermal resistance, but these approaches run contrary to miniaturization. Unfortunately, many designs have already taken advantage of heat dissipating measures. Alternatively, we can specify longer life times for standard 85°C rated capacitors. Aluminium electrolytic capacitors have been widely used in the electronic industry. Failure mechanism of aluminium electrolytic capacitors due to thermal overstress has been studied.

2.0 Aluminum Electrolytic Capacitor

As shown in Fig. 1 [2], an aluminum electrolytic capacitor consists of a cathode aluminum foil, electrolytic paper, electrolyte, and an aluminum oxide layer on the anode foil surface, which acts as the dielectric. When in contact with the electrolyte, the oxide layer possesses an excellent forward direction insulation property (Bengt, 1995). To get higher capacitance values for the same surface area of the anode and cathode foils, the foil is etched by a chemical process. Together with magnified effective surface

area attained by etching the foil, high capacitance value is obtained in a small volume (Fife, 2006). Since the oxide layer has rectifying properties; a Capacitor has polarity. If both the anode and cathode foils have an oxide layer, the capacitors would be bipolar. Here, analysis of non-solid aluminum electrolytic capacitors, in which the electrolytic paper is impregnated with a liquid electrolyte, has been done. After the paltes are etched, they are anodized by coating themwith a thin aluminum oxide layer on the surface of the foil. This layer of aluminumoxide actsas the dielectric (insulator) and serves to block the flow of direct current between the two capacitor plates. Figure 2 and Figure 3 showsDB series type Keltron Electrolytic Capacitor that was used for the study.

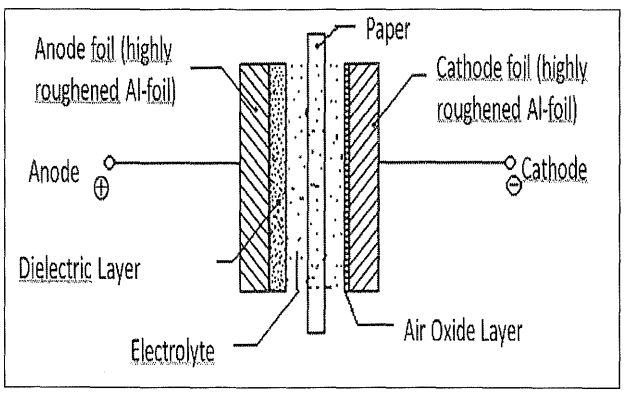

Fig. 1. Internal structure of Aluminium electrolytic capacitor [1].

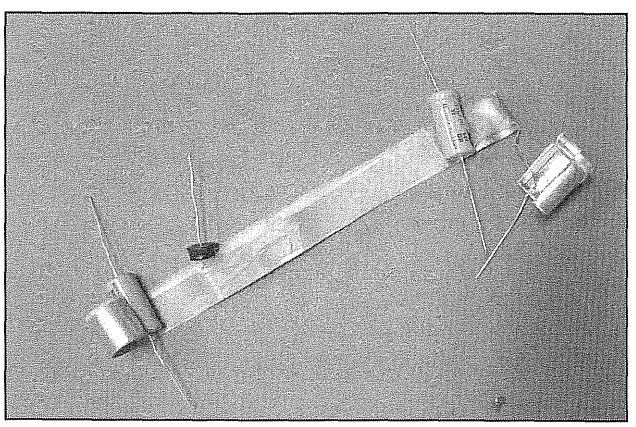

Fig. 2. Cathode of DB series Keltron Aluminium Electrolytic Capacitor.

Source: Photo taken at Life Cycle Reliability Engineering Laboratory, RRSD, BARC Mumbai.

3.0 Equivalent Circuit of Aluminium Electrolytic Capacitor

A simplified electrical lumped parameter model of impedance, M1, defined for an electrolytic capacitor is shown in Figure 4. The ESR dissipates some of the

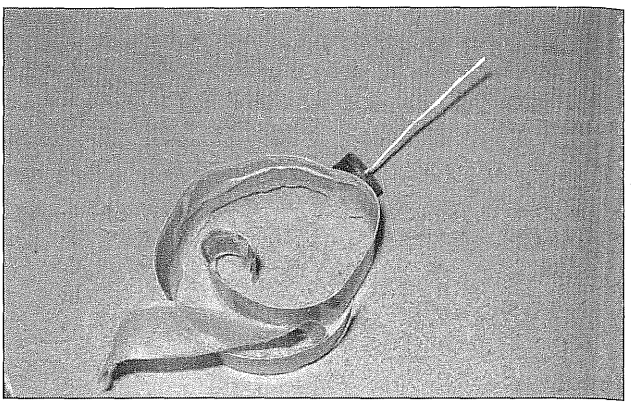

Fig. 3. Anode of DB series Keltron Aluminium Electrolytic Capacitor Source: Photo taken at Life Cycle Reliability Engineering Laboratory, RRSD, BARC Mumbai.

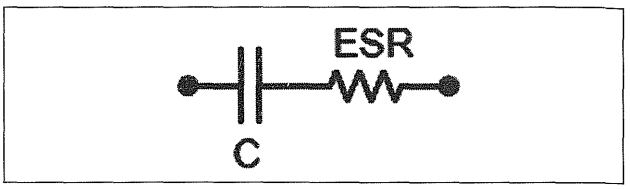

Fig. 4. Lumped parameter model (M1)

stored energy in the capacitor. An ideal capacitor would offer no resistance to the flow of current at its leads.

It has been observed that under thermal overstress storage conditions (Bengt, 1995; J. Celaya et al., 2011a), the capacitance (C) and ESR value depends of the electrolyte resistance RE.A more detailed lumped parameter model derived for an electrolytic capacitor under thermal overstress condition, M2 can be modified from M1, as shown in Figure 5. R_1 is the combined series and parallel resistances in the model. RE is the electrolyte resistance. The combined resistance of R_1 and R_E is the ESR of the capacitor. C is the total capacitance of the capacitor.

4.0 Failure Analysis of Aluminium Electrolytic Capacitor

The following two conditions must be considered in defining "failure".

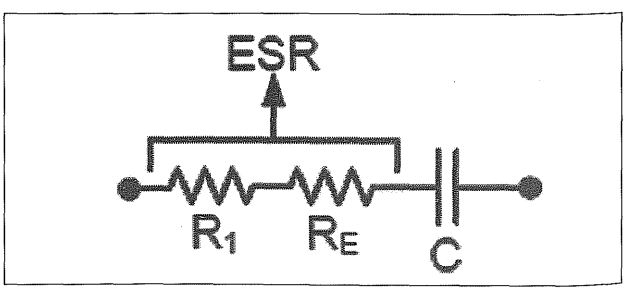

Fig. 5. Lumped parameter model (M2)

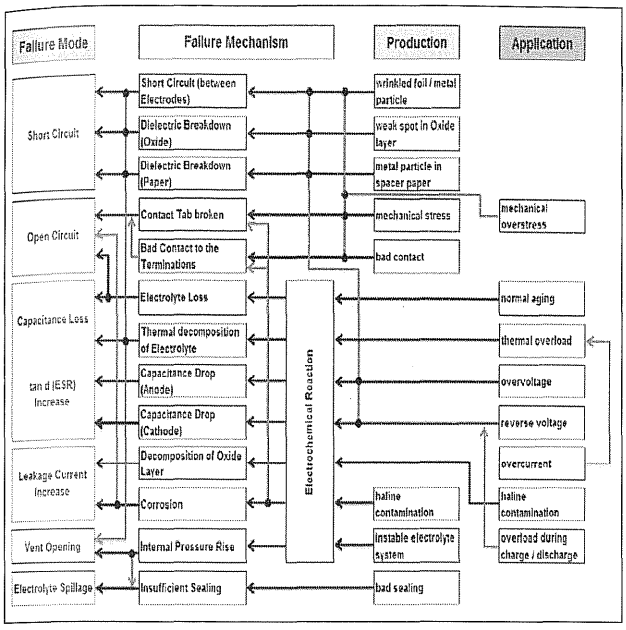

Fig. 6. Failure modes and mechanisms of aluminium electrolytic capacitor

a) Catastrophic Failure:

When a capacitor has completely lost his functions due to a short or open circuit.

b) Degradation Failure:

The gradual degradation of a capacitor. In the case of a degradation failure, the criteria for failure differ according to the use of a capacitor. Capacitor requirements vary depending upon the type of the finished products. Therefore, the specified value in the specification is used as the judging criteria.

Figure 6 and Figure 7 shows different types of failure modes and mechanisms of aluminium electrolytic capacitor [6].

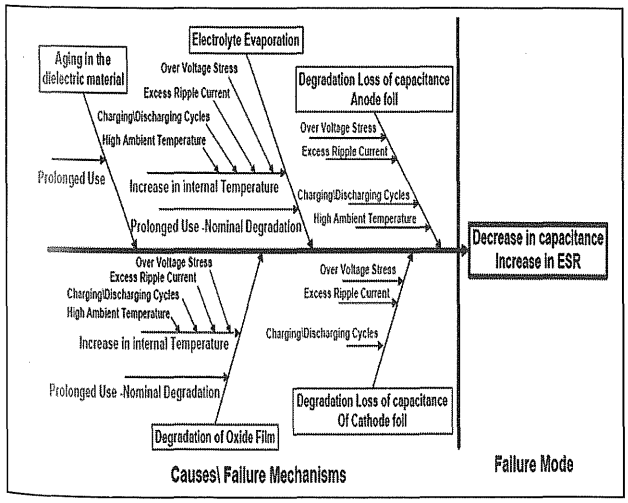

Fig. 7. Fishbone structure of failure mechanism of aluminium electrolytic capacitor

5.0 Structural Model of Capacitor

For deriving the physics based models of an electrolytic capacitor it is also necessary to know about the structural and manufacturing details, since health estimations are done based on the type of electrolyte, volume of electrolyte, oxide layer thickness etc. The models defined use this information for making effective degradation/failure predictions [6]. A detail structural study of the electrolytic capacitor under test is discussed in this section. During modelling it is not possible to know the exact amount of electrolyte present in a capacitor. But using information from the structural details as shown in Figure 8, we can approximately calculate the amount of electrolyte present. A very highly porous separator paper is used which soaks all the electrolyte. The paper separator is sandwiched between anode and cathode, each having a thickness dS, dA and dC respectively (dS ~ dA ~ dC). Based on the type and configuration, the electrolyte volume will vary which can be updated in the model parameters. The equation for calculating the approximate electrolyte volume is derived from calculating the total capacitor capsule volume, Vc given by:

$$Vc = \pi * r_c^2 * h_c, \quad (1)$$

Where:

rc = radius of capacitor capsule

hc = height of capacitor capsule

The approximate electrolyte volume, Ve based on all the other known structural details of the capacitor can be expressed as:

$$V_e = \pi * r_c^2 * h_c - A_s(d_A + d_C) \quad (2)$$

6.0 Degradation Model of Capacitor

Exposure to high temperatures, T applied > T rated results in accelerated aging of capacitors (Kulkarni, Celaya, et al., 2011; J. Celaya et al., 2011a; 60068-1, 1988). Higher ambient storage temperature accelerates the rate of electrolyte evaporation leading to degradation of the capacitance (Kulkarni, Celaya,

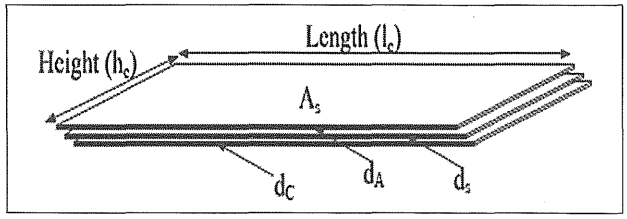

Fig. 8. Open structure of capacitor

et al., 2011; Bengt, 1995). The depletion in electrolyte volume, Ve, (Kulkarni, Biswas, et al., 2011; Rusdi et al., 2005) is given by:

$$V_e(t) = V_0 - (A_s j_{e0} w_e) * t \quad (3)$$

Where:

V_0= initial electrolyte volume

J_{eo}= evaporation rate

w_e= volume of ethyl glycol molecule

t = time in hours.

The total lumped capacitance from first principles of electromagnetism is given by:

$$C = (2\epsilon_R \epsilon_0 A_s)/d_C \quad (4)$$

Where:

ε_R= relative dielectric constant

ε_O= permittivity of free space

Thus from Eq. (3) and Eq. (4) we can derive the first principles capacitance degradation model, M3 given by:

$$M_3 : C(t) = \left(\frac{2\epsilon_R \epsilon_0}{d_C}\right)\left(\frac{V_0 - V_e(t)}{j_{eo}\, t\, w_e}\right) \quad (5)$$

As discussed earlier, increase in the core temperature evaporates the electrolyte thus decreasing the electrolyte volume leading to degradation in capacitance. The resultant decrease in the capacitance can be computed using model, M3 wherein the decrease in electrolyte volume, (Ve) leads to decrease in capacitance, (C).

The flow of current during the charge and discharge cycle of the capacitor causes the internal temperature to rise. The excess heat results in a rise in the internal temperature of the electrolyte.

7.0 Thermal Overstress Experiment

On increasing the temperature of the surrounding, the temperature of core region of capacitor increases leading to the evaporation of the electrolyte.

In the experimental set-up, high temperature storage conditions for capacitor were simulated, where a single capacitor was placed in a controlled chamber and the temperature was raised above their rated specification. Keltron DB series Aluminium electrolytic capacitors were taken from the same lot rated for 63V and maximum storage temperature rating of 85^{0}C. Experiments were conducted with 220 µF capacitors with TOS temperature at 115^{0}C. The chamber temperature was gradually increased in steps of 25^{0}C till the pre-determined temperature limit was reached. The capacitors were allowed to settle at a set temperature for 15 min and then the next step increase was applied. This process was continued till the required temperature limit was attained. To decrease possibility of shocks due to sudden decrease in the temperature, the above procedure was followed. At the end of specific time interval, the temperature was lowered in steps of 25^{0}C till the required room temperature was reached. Before being characterized, the capacitors were kept at room temperature for 15 min.

The ESR, Capacitance and ESL value were measured through the Wayne Kerr make Impedance Analyzer.

8.0 Experimental Setup

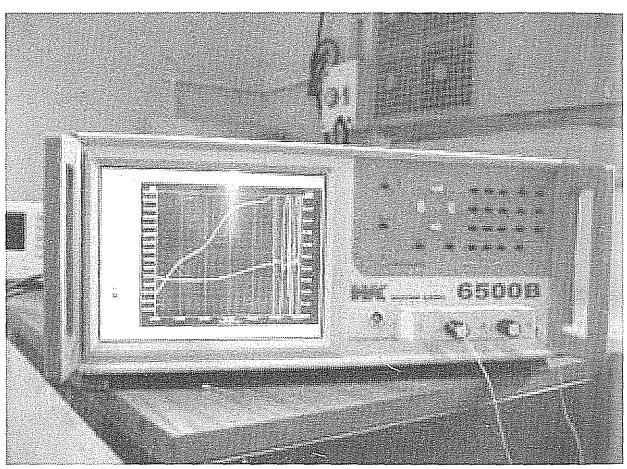

Fig. 9. Wayne Kerr 6500B Impedance Analyzer

Source: Photo taken at Life Cycle Reliability Engineering Laboratory, RRSD, BARC Mumbai.

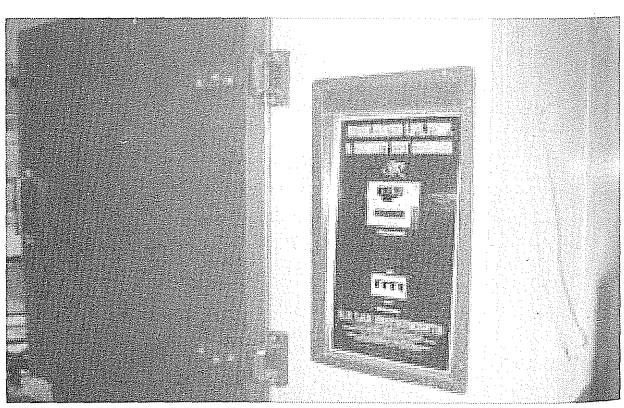

Fig. 10. Accelerated life, Temperature and Humidity Chamber

Source: Photo taken at Life Cycle Reliability Engineering Laboratory, RRSD, BARC Mumbai.

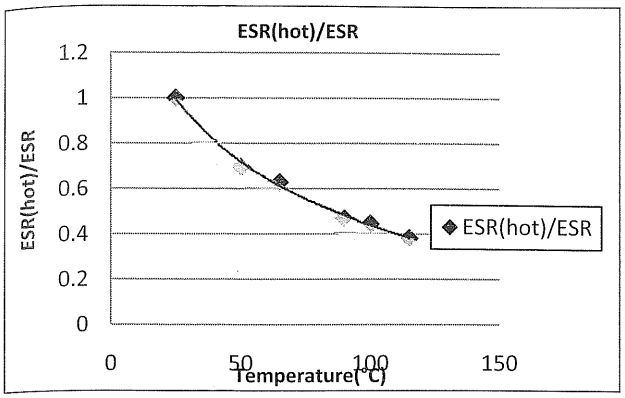

Fig. 11. Plot of ESR with temperature

9.0 Observations and Results

The DB series Keltron Aluminium electrolytic capacitor was initially heated from room temperature.

Table 1

Temperature (°C)	Capacitance value (μF)	ESR value (mΩ)	ESR(hot)/ ESR
25	230.19	97.751	1
50	235.92	68.083	0.696
65	236.92	61.42	0.628
90	242.23	45.642	0.467
100	245.48	43.561	0.445
115	251.43	37.336	0.381

From figure 11, it is observed that the ESR (effective series resistance) decreases with the increase in temperature. It is because, with the increase in the temperature the conductivity of the electrolyte increase, which leads to the decrease in the ESR.

Conducting wires were connected in the cathode and anode of the aluminium electrolytic capacitor. The capacitor was kept inside the Accelerated life, Temperature and Humidity Chamber as shown in Figure 10, and the temperature was settled at 115^{0}C. The wires were taken out from the Accelerated life, Temperature and Humidity Chamber and were connected to the Wyane Kerr Impedance analyzer as shown in Figure 9. The capacitance was measured through Wyane Kerr Impedance analyzer. Following observations was taken:

From Table 2, it is observed that the capacitance value decreases due to thermal overstress.

10. Conclusion

If the aluminium electrolytic capacitor is subject to thermal overstress for a longer period of time,

Table 2

Temperature (in ^{0}C)	Time (in hours)	Capacitance Value (in μF)
115	0	254.65
115	20	253.60
115	40	253.18
115	60	253.05
115	80	252.87
115	120	252.32

the capacitance will decrease, whereas the ESR will increase. This is because; when the capacitor is subjected to thermal overstress the electrolyte of the capacitor starts to evaporate. Hence the conductivity decreases which leads to the decrease in capacitance and increase in the ESR value. The behaviour of the aluminium electrolytic capacitor with thermal overstress was validated from the above experiment. A life model of Aluminium electrolytic capacitors has been developed that is based on the primary wear-out mechanism of electrolyte vaporization and loss through the end seal. The model incorporates relationships for ESR change with electrolyte loss, ESR change with temperature, and heat transfer value with geometric dimensions.

References

1. J. L. Stevens, J. S. Shaffer, and J. T. Vandenham, "The service life of large aluminium electrolytic capacitors: effects of construction and application, "in *Conf. Rec. IEEE-IAS Annu. Meeting*, vol. 3, 2001, pp.2493–2499.
2. Dr. Arne Albertsen, "Electrolytic Capacitor Lifetime Estimation", in JIANGHAI EUROPE GmbH, 2010.
3. Bengt, A. (1995). Electrolytic capacitors theory and applications. RIFA Electrolytic Capacitors.
4. Celaya, J., Kulkarni, C., Biswas, G., & Goebel, K. (2011a). A model-based prognostics methodology for electrolytic capacitors based on electrical overstress accelerated aging. Proceedings of Annual Conference of the PHM Society, September 25-29, Montreal, Canada.
5. Fife, J. (2006, August). Wet electrolytic capacitors (Patent No: 7,099 No. 1). Myrtle Beach, SC: AVX Corporation.
6. Kulkarni, C. S., Celaya, J. R., Goebel, K., Biswas, G. (2012, September). Bayesian Framework Approach for Prognostic Studies in Electrolytic Capacitor under Thermal Overstress Conditions.
7. Kulkarni, C., Biswas, G., Celaya, J., & Goebel, K. (2011). A case study for capacitor prognostics under accelerated degradation. IEEE 2011 Workshop on Accelerated Stress Testing & Reliability (ASTR), September 28-30,San Francisco, CA.
8. Rusdi, M., Moroi, Y., Nakahara, H., & Shibata, O. (2005).Evaporation from water ethylene glycol liquid mixture. Langmuir - American Chemical Society, 21 (16), 7308- 7310.

Life Cycle Reliability and Safety Engineering
Vol.5 Issue 2 (2016) 20-31

Reliability Estimation of *m−out−of−n: G* Standby Systems Using Fourth Order Runge−Kutta Algorithm

M. Boopathi[1], R. Sujatha[2], C. Senthil Kumar[3], S. Narasimman[4]
[1,2,4] *Department of Mathematics, SSN College of Engineering, Kalavakkam, Tamil Nadu*
[3] *Safety Research Institute, Atomic Energy Regulatory Board, Kalpakkam, Tamil Nadu*
[1] *rithishboopathi@gmail.com*

Abstract

Reliability models based on the concepts of Markov Chain is extensively applied in various fields. Standby techniques are used to improve system availability. The components in standby systems are assumed to be mutually independent. But standby systems having different failure rates and repair rates, in such cases all the components of standby systems cannot be treated as identical. In this paper, we propose a general scenario for computing availability and reliability for *m−out−of−n:G* standby systems using fourth order Runge−Kutta (R−K) algorithm. The state dependent system is converted into a systems of first ordinary differential equations and then Runge−Kutta algorithm is applied to estimate the reliability of this *m−out−of−n:G* standby systems. An illustration for *3−out−of−4:G* warm standby system and a case study for *1−out−of−2, 1−out−of−3, 2−out−of−3, 2−out−of−4,* diesel generator (DG) configurations are presented. This proposed method provides accurate solution close to analytic solution obtained by Laplace transform techniques.

Keywords: Fourth order Runge−Kutta method; m−out−of−n:G standby system; Laplace transform; reliability of standby system; m−out−of−n:DG Configurations.

1. Introduction

Markov analysis looks at a system being in one of the several states. The fundamental assumption in Markov process is that the probability that a system will undergo a transition from one state to another state depends only on the current state of the system and not on any previous state the system may have experienced. In Markov analysis, we assume that each of the n components will be in one of two states namely operating or failed [1]. In this paper, $m-out-of-n:G$ standby system is discussed. Markov model has been generally applied to the quantification of system reliability, unavailability at given time points and to the problem of estimating nuclear power station blackout as a function of blackout duration. Station blackout (SBO) is defined as the loss of all AC power to the essential and non essential electrical buses in a nuclear power plant (NPP). Since nuclear plants derive power from several offsite power and emergency Diesel Generators (DG), station blackout (SBO) involves the loss of both the power and onsite emergency DG power [9]. In this paper, the reliability of this DG configuration has been quantified by RungeKutta method. Here, 1−out−of−2, 1−out−of−3, 2−out−of−3, 2−out−of−4, DG configurations are discussed and reliability obtained by R-K method.

The structure of the paper is organized in the following way: Section 2 contains basic concepts for $m-out-of-n:G$ standby systems. Proposed approach for estimating the reliability for $m-out-of-n:G$ standby system using fourth order Runge−Kutta algorithm is presented in section 3. General scenario of $m-out-of-n:G$ standby system is discussed in section 4. In section 5, an illustration $3-out-of-4:G$ warm standby system is discussed. Case study for estimating the reliability of DG configurations and unavailability is debuted in section 6, conclusions are presented in section 7.

2. General Concepts of *m−out−of−n : G* standby system

The general $m-out-of-n:G$ standby systems have important characteristics as follows: for such a system, when an operating component fails, a standby component becomes active and the system is working if at least m components are in operation. There are three types in component standby that is cold, hot and warm standby. Cold standby implies that inactive components have zero failure rates. Hot

The authors thank Atomic Energy Regulatory Board India (Project No: AERB/CSRP/53/06/2013) for providing financial assistance to carry out this work.

standby implies that an inactive component has same failure rate as when it is in operation. Warm standby implies that an inactive component has a failure rate between cold and hot, it is also called dormant failure. This type of system have been used in several research fields including medical diagnosis, redundant system testing, power plant system, etc., In this system, the components in standby system are assumed to be statistically identical and independent. But in standby system having different failure and repair rates, all the components of the standby systems cannot be treated as identical. Here, $3-out-of-4:G$ warm standby systems are studied and it operates as two category of components, component is of type-I and component of type-II. Components of type-I having low failure rate and preferably repaired if there is one failed. The general scenario for $m-out-of-n:G$ standby system based on Markov Chain approach for estimating reliability using Runge Kutta algorithm is presented. An illustration for $3-out-of-4:G$ warm standby system and a case study for *1-out-of-2, 1-out-of-3 and 2-out-of-3, 2-out-of-4,* DG configurations are discussed.

3. Proposed Approach

Reliability of state dependent system is computed using fourth order Runge-Kutta algorithm. In order to calculate reliability, availability these systems are converted into system of first order ordinary differential equations. The system of first order ordinary differential equations derived is solved using fourth order Runge-Kutta algorithm; this method provides an accurate reliability value for any type of state dependent systems which satisfy the concept of Markov Chain.

3.1 Runge-Kutta Algorithm for Reliability of *m-out-of-n : G* standby system

Runge-Kutta algorithm for fourth order method is a numerical technique used to solve ordinary differential equation of the form $\frac{dY}{dx}=f(x,Y)$, with initial condition $Y(x_0)=Y_0$. The Runge-Kutta method of fourth order is given by

$$Y_{n+1}=Y_n+\frac{h}{6}(k_1+2k_2+2k_3+k_4)$$

$$where \quad k_1=f(x_n,Y_n), \qquad k_2=f\left(x_n+\frac{h}{2},Y_n+\frac{k_1}{2}\right)$$

$$k_3=f\left(x_n+\frac{h}{2},Y_n+\frac{k_2}{2}\right), \qquad k_4=f(x_n+h,Y_n+k_3)$$

This formula is applied to calculate reliability values. The vector version of Runge-Kutta method can be revised as follows

$$P_{n+1}=P_n+\frac{1}{6}(k_1+2k_2+2k_3+k_4)$$

$$where \quad k_1=h*P_n*Q, \qquad k_2=h*\left(P_n+\frac{k_1}{2}\right)*Q,$$

$$k_3=h*\left(P_n+\frac{k_2}{2}\right)*Q, \qquad k_4=h*(P_n+k_3)*Q$$

Where Q is the rate transition matrix, P_n is the initial probability vector, h is the step size. $O(h^5)$ is the order of truncation error. Runge-Kutta method has advantage of high precision and good rate of convergence, and variable step size in computation [3], [6]. The pseudo code is given by.

$$\begin{aligned}
&select \;\; P_0; \;\; P \leftarrow P_0;\\
&t \leftarrow 0; \;\; t \leftarrow 0; \;\; select \; h;\\
&while \;\; t< T\\
&k_1 \leftarrow h*Q*P; \qquad k_2 \leftarrow h*Q*\left(P+\frac{k_1}{2}\right);\\
&k_3 \leftarrow h*Q*\left(P+\frac{k_2}{2}\right); \qquad k_4 \leftarrow h*Q*(P+k_3);\\
&P \leftarrow P+\frac{1}{6}(k_1+2k_2+2k_3+k_4);\\
&t \leftarrow t+h; \qquad i \leftarrow i+1;
\end{aligned} \tag{1}$$

Where P is the initial probability vector, i *and* T represents the iteration count and stopping criteria respectively.

4. General Scenario of *m-out-of-n : G* Standby System

Markov transition diagram is a powerful technique to analyze system states and obtain the availability of a repairable system. To give a clear prediction for state transitions of the system, an $m-out-of-n:G$ standby system with identical component as a general case, which satisfies the following conditions is considered [7], [8].

1.1 The system consists of n identical components with operation failure rate λ, dormant failure rate $\overline{\lambda}$ in case of warm standby and repair rate μ. In case of hot standby an inactive component has same failure rate as when it is in operation.

2.1 The redundant configuration has $m(\leq n)$ principal components.

3.1 There are r repair facilities available. At most, r $(r \geq 1)$ components can be repaired at a time.

4.1 Reliability of *m-out-of-n : G* Stand by Redundant Configuration

The state transition diagram for this

$m-out-of-n:G$ standby redundant configuration is displayed in Fig. 1.

Let $P_i(t)$ represent the probability that system is in state i at time t, and let $P_i'(t)$ denotes the derivative of $P_i(t)$. $R(t)$, $A(t)$ and MTTF denotes respectively reliability, availability and Mean Time To Failure of the system. $\lambda, \bar{\lambda}, \mu$ denotes the system failure rate, dormant (standby) failure rate and repair rate respectively.

Let $P_1'(t), P_2'(t), \cdots, P_n'(t), \forall i = 1,2,\cdots,n$ be the derivatives of the probabilities $P_1(t), P_2(t), \cdots, P_n(t), \forall i = 1,2,\cdots,n$ respectively [1], [2].

According to the state transition rule the first order differential equations become,

$$\begin{aligned} P_i'(t) &= (inflow\ to\ state\ i) - (outflow\ from\ state\ i) \\ &= \sum_{j \neq i} [rate\ of\ transition\ to\ state\ i\ from\ state\ j] \\ &\quad \times (probability\ of\ state\ j) - \\ &\quad \sum_{j \neq i} [rate\ of\ transition\ to\ state\ i\ from\ state\ j] \\ &\quad \times (probability\ of\ state\ i) \end{aligned} \tag{2}$$

Then

$$\begin{aligned} P_0'(t) &= -\lambda_0 P_0(t) + \mu_1 P_1(t) \\ &\vdots \\ P_k'(t) &= \lambda_{k-1} P_{k-1}(t) - (\lambda_k + \mu_k) P_k(t) + \mu_{k+1} P_{k+1}(t) \\ &\vdots \\ P_n'(t) &= \lambda_{n-1} P_{n-1}(t) - \mu_n P_n(t) \end{aligned}$$

$$\begin{bmatrix} P_0'(t) \\ \vdots \\ P_k'(t) \\ \vdots \\ P_n'(t) \end{bmatrix} = \begin{bmatrix} -\lambda_0 & \mu_1 & 0 & 0 & 0 & 0 & 0 & 0 & 0 \\ \vdots & \vdots & \vdots & \vdots & \vdots & \vdots & \vdots & \vdots & \vdots \\ 0 & 0 & \cdots & \lambda_{k-1} & -(\lambda_k+\mu_k) & \mu_{k+1} & \cdots & 0 & 0 \\ \vdots & \vdots & \vdots & \vdots & \vdots & \vdots & \vdots & \vdots & \vdots \\ 0 & 0 & \cdots & 0 & 0 & 0 & \cdots & \lambda_{n-1} & -\mu_n \end{bmatrix} \begin{bmatrix} P_0(t) \\ \vdots \\ P_k(t) \\ \vdots \\ P_n(t) \end{bmatrix} \tag{3}$$

where k represents number of components under repair.

$$\lambda_k = m\lambda + (n-m-k)\bar{\lambda},\ for\ k = 0,1,\cdots,n-m$$
$$\lambda_k = (n-k)\lambda,\ for\ k = n-m+1,\cdots,n-1$$
$$\mu_k = \min\{r,k\} \times \mu,\ for\ k = 1,2,\cdots,n$$

By the concepts of first order ordinary differential equation $\frac{dP(t)}{dt} = Q\,P(t)$ with initial conditions $P(0) = [1\ 0\ 0 \cdots 0]^T$, where Q represents the rate transition matrix of $m-out-of-n:G$ system.

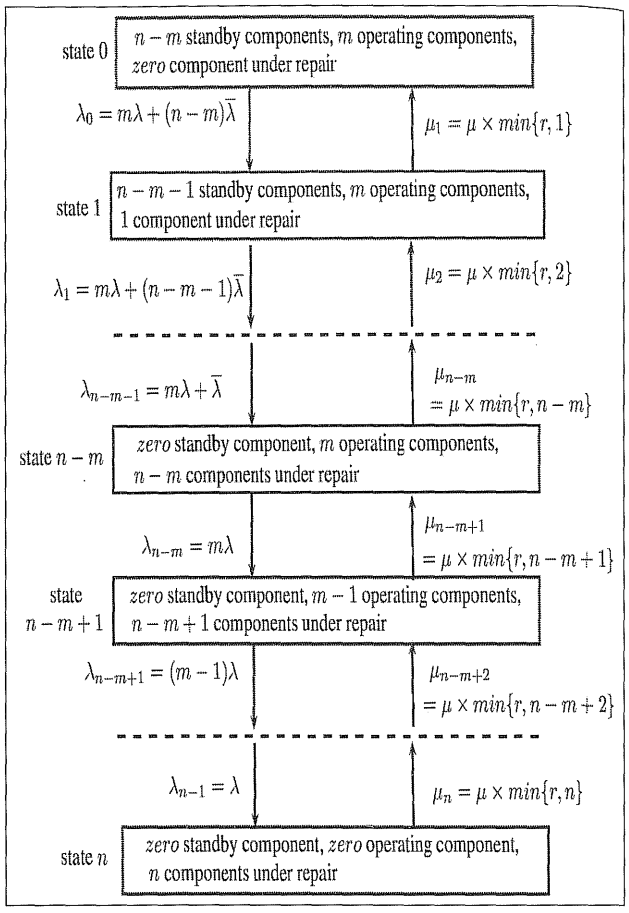

Fig. 1. General Markov structure of $m-out-of-n:G$ standby system

4.2 Calculation Mean Time To Failure of $m-out-of-n:G$ Standby Systems

Let $P(t) = [P_1(t)\ P_2(t) \cdots P_n(t)]^T$, $P(\infty) = [0\ 0\ 0 \cdots 0]^T$ $P(0) = [1\ 0\ 0 \cdots 0]^T$ *and* $P(\infty) - P(0) = [-1\ 0\ 0 \cdots 0]^T$ then the matrix representation of the MTTF is given by,

$$\begin{bmatrix} -1 \\ \vdots \\ 0 \\ \vdots \\ 0 \end{bmatrix} = \begin{bmatrix} -\lambda_0 & \mu_1 & 0 & 0 & 0 & 0 & 0 & 0 & 0 \\ \vdots & \vdots & \vdots & \vdots & \vdots & \vdots & \vdots & \vdots & \vdots \\ 0 & 0 & \cdots & \lambda_{k-1} & -(\lambda_k+\mu_k) & \mu_{k+1} & \cdots & 0 & 0 \\ \vdots & \vdots & \vdots & \vdots & \vdots & \vdots & \vdots & \vdots & \vdots \\ 0 & 0 & \cdots & 0 & 0 & 0 & \cdots & \lambda_{n-1} & -\mu_n \end{bmatrix} \begin{bmatrix} q_0 \\ \vdots \\ q_k \\ \vdots \\ q_n \end{bmatrix}$$

Where $[q_0\ q_2 \cdots q_k \cdots q_n]^T$ is an arbitrary vector [4], [5]. Solving the system we get the vectors $q_0, q_2, \cdots, q_n$ and the mean time to failure is $MTTF = q_0 + q_2 + \cdots + q_n$..

5. Illustration.

The proposed approaches have been applied to $3-out-of-4:G$ warm standby system. The results obtained by applying Runge–Kutta algorithm are

compared with analytic solution of Laplace transform techniques.

The non-identical components of $3-out-of-4:G$ warm standby systems consists of four components or elements A, B, C *and* D. These components are divided into two types namely, type–I and type–II. Type–I components consists of A, B elements and type II consists of components C *and* D elements. In $3-out-of-4:G$ warm standby system each states, $\vee, \Theta, \times$ represents operating, standby, failure of components respectively. $\times_i$ $(i=1,2,3,4)$ denotes a component in the i^{th} failed state. State 1 for example, means only one component of type–I is in operation and other is in the standby; and the two components of type–II are all in operation. State 2 means there is only one component of type–I in failure and other components are all in operation. And it is similar to state 4 where there is only one component of type–II in failure. The other states, are given in similar way.

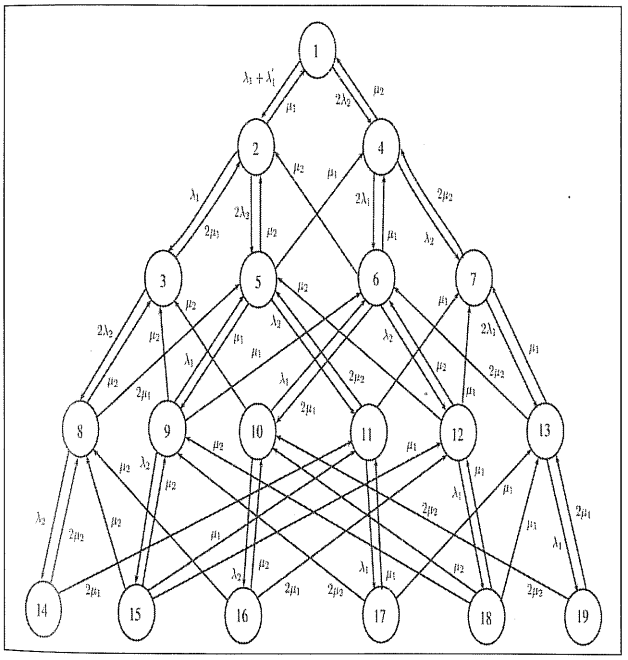

Fig. 2. Markov Chain based 3–out–of–4 : G warm standby system

Taking state 5 for example where the left rectangle in the up line means elements A *and* C can be operation while element B failed first and D second, the right rectangle in the up line means A *and* D can be operation while B and D under repair and B failed first and C second respectively; in addition,the meaning for the other two rectangles in the low line can be readily obtained in a similar way.

The failure rates are λ_1, λ_2 and repair rates are μ_1, μ_2. Let λ_1' be the inactive failure rates. The behavior

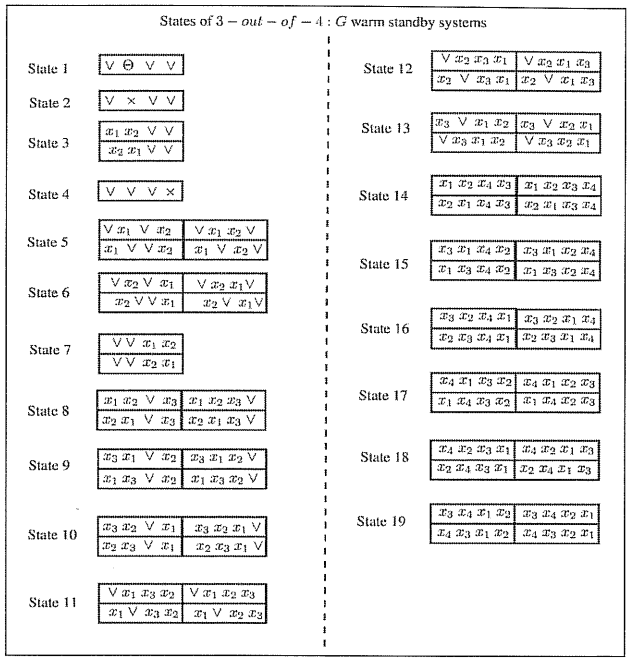

Fig. 3. Markov Chain of states corresponding to the 3–out–of–4:G warm standby system

of working procedure and transition between the states are shown Fig. 2,

The states corresponding to the nodes reduced is presented in detail as depicted in Fig. 3,

From *3–out–of–4:G* warm standby system is modeled in Fig. 2, and the corresponding state transition rules provides a set of system of first order ordinary differential equation [7]. We can reduce this set of equations according to Fig. 2, we have set of system of differential equations (4)-(12) as follows

$$P_1 = P_1(t) \tag{4}$$
$$P_2 = P_2(t) \tag{5}$$
$$P_3 = P_3(t) \tag{6}$$
$$P_4 = P_4(t) \tag{7}$$
$$P_5 + P_6 = P_5(t) \tag{8}$$
$$P_7 = P_7(t) \tag{9}$$
$$P_8 + P_9 + P_{10} = P_6(t) \tag{10}$$
$$P_{11} + P_{12} + P_{13} = P_8(t) \tag{11}$$
$$P_{14} + P_{15} + P_{16} + P_{17} + P_{18} + P_{19} = P_9(t) \tag{12}$$

Using Fig. 3, all states of aggregate ones are combined as in Fig. 4, and reduced system of equations (13)-(21) is given below.

$$P_1'(t) = -(\lambda_1 + \lambda'_1 + 2\lambda_2)P_1(t) + \mu_1 P_2(t) + \mu_2 P_4(t) \tag{13}$$
$$P_2'(t) = (\lambda_1 + \lambda'_1)P_1(t) - (\lambda_1 + 2\lambda_2 + \mu_1)P_2(t) + 2\mu_1 P_3(t) + \mu_2 P_5(t) \tag{14}$$

$$P_3'(t) = \lambda_1 P_2(t) - 2(\lambda_2 + \mu_1)P_3(t) + \mu_2 P_6(t) \quad (15)$$

$$P_4'(t) = 2\lambda_2 P_1(t) - (2\lambda_1 + \lambda_2 + \mu_2)P_4(t) + \mu_1 P_5(t) + 2\mu_2 P_7(t) \quad (16)$$

$$P_5'(t) = 2\lambda_2 P_2(t) + 2\lambda_1 P_4(t) - (\lambda_1 + \lambda_2 + \mu_1 + \mu_2)P_5(t) + 2\mu_1 P_6(t) + 2\mu_2 P_8(t) \quad (17)$$

$$P_6'(t) = 2\lambda_2 P_3(t) + \lambda_1 P_5(t) - (\lambda_2 + 2\mu_1 + \mu_2)P_6(t) + 2\mu_2 P_9(t) \quad (18)$$

$$P_7'(t) = \lambda_2 P_4(t) - 2(\lambda_1 + \mu_2)P_7(t) + \mu_1 P_8(t) \quad (19)$$

$$P_8'(t) = \lambda_2 P_5(t) + 2\lambda_1 P_7(t) - (\lambda_1 + \mu_1 + 2\mu_2)P_8(t) + 2\mu_1 P_9(t) \quad (20)$$

$$P_9'(t) = \lambda_2 P_6(t) + \lambda_1 P_8(t) - 2(\mu_1 + \mu_2)P_9(t) \quad (21)$$

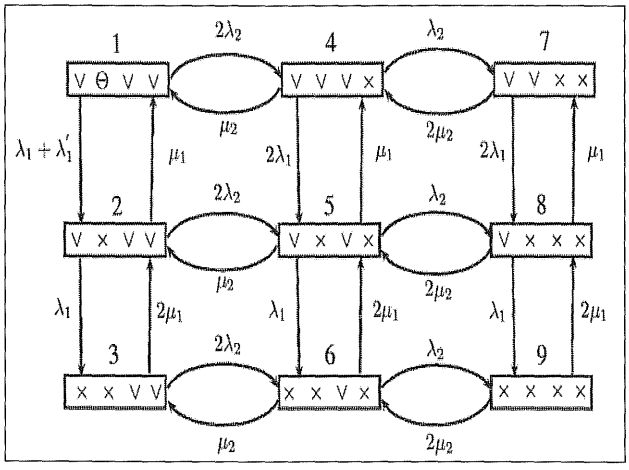

Fig. 4. Combined Markov transition diagram for 3-out-of-4:G warm standby system.

with initial condition $[P_1(0)\ P_2(0) \cdots P_9(0)] = [1\ 0\ 0 \cdots 0]$ and $\sum_{i=1}^{9} P_i(t) = 1$. To calculate the component reliabilities $P_1(t) + P_2(t) \cdots, P_9(t)$ using fourth order Runge-Kutta algorithm as explained in section 3.

From Fig. 4, it is known that the system is in operation when it is in one of states 1,2,4. Hence, general form of the availability of the system is given by (13)-(21)

$$A(t) = P_1(t) + P_2(t) + P_4(t) \quad (22)$$

The Laplace transform technique applied to equations (13)-(21) becomes tedious. Based on the above analysis, if all the failure states of the system are regarded as absorbing states we have the following set of first order ordinary differential equation is,

$$P'_1(t) = -(\lambda_1 + \lambda'_1 + 2\lambda_2)P_1(t) + \mu_1 P_2(t) + \mu_2 P_4(t) \quad (23)$$

$$P'_2(t) = (\lambda_1 + \lambda'_1)P_1(t) - (\lambda_1 + 2\lambda_2 + \mu_1)P_2(t) + 2\mu_1 P_3(t) + \mu_2 P_5(t) \quad (24)$$

Table 1 Reliability of R-K Solutions Versus Laplace Solution for 3-out-of-4 : G Warm Standby System

S. No	Time *t*-values	*R-K* Method Solutions	Laplace Transform Technique Solutions
1	0	0.9799	1.00000
2	100	0.9305	0.97998
3	200	0.8637	0.93046
4	300	0.7882	0.86368
5	400	0.7099	0.78827
6	500	0.6328	0.70997
7	600	0.5593	0.63283
8	700	0.4908	0.55929
9	800	0.4282	0.49083
10	900	0.3717	0.42820
11	1000	0.3213	0.37171
12	1100	0.2767	0.32127
13	1200	0.2374	0.27664
14	1300	0.2033	0.23745
15	1400	0.1735	0.20323
16	1500	0.1477	0.17350
17	1600	0.1256	0.14780
18	1700	0.1066	0.12564
19	1800	0.0904	0.10663
20	1900	0.0765	0.09035
21	2000	0.0646	0.07644
22	2100	0.0545	0.06459
23	2200	0.0459	0.05452
24	2300	0.0387	0.04597
25	2400	0.0326	0.03872
26	2500	0.0274	0.03259
27	2600	0.0230	0.02741
28	2700	0.0193	0.02304
29	2800	0.0163	0.01934
30	2900	0.0136	0.01623
31	3000	0.0114	0.01362
32	3100	0.0095	0.01142
33	3200	0.0080	0.00957
34	3300	0.0067	0.00802
35	3400	0.0057	0.00671
36	3500	0.0047	0.00562
37	3600	0.0039	0.00471
38	3700	0.0033	0.00394
39	3800	0.0027	0.00323
40	3900	0.0023	0.00275
41	4000	0.0019	0.00230

$$P'_4(t) = 2\lambda_2 P_1(t) - (2\lambda_1 + \lambda_2 + \mu_2)P_4(t) + \mu_1 P_5(t) + 2\mu_2 P_7(t) \quad (25)$$

The above differential equations (23)-(25) is written in the form

$$\begin{bmatrix} P_1'(t) \\ P_2'(t) \\ P_4'(t) \end{bmatrix} = \begin{bmatrix} -(\lambda_1+\lambda'_1+2\lambda_2) & \mu_1 & \mu_2 \\ (\lambda_1+\lambda'_1) & -(\lambda_1+2\lambda_2+\mu_1) & 0 \\ 2\lambda_2 & 0 & -(2\lambda_1+\lambda_2+\mu_2) \end{bmatrix} \begin{bmatrix} P_1(t) \\ P_2(t) \\ P_4(t) \end{bmatrix} \quad (26)$$

The above system is of the form $\frac{dP(t)}{dt} = Q\,P(t)$ with initial conditions $[P_1(0)\ P_2(0)\ P_4(0)] = [1\ 0\ 0]$, where Q represents the rate transition matrix. The reliability of $3-out-of-4:G$ warm standby system is given by

$$R(t) = A(t) = P_1(t) + P_2(t) + P_4(t) \quad (27)$$

If all repair rates $\mu_1 = 0\ and \mu_2 = 0$ in equations (23)-(25), the analytical solution of the system reliability using Laplace transform technique we have

$$R(t) = \left(1+\frac{\lambda_1}{\lambda'_1}\right)e^{-(\lambda_1+2\lambda_2)t} - \left(\frac{2\lambda_2}{\lambda_1-\lambda'_1-\lambda_2}\right)e^{-(2\lambda_1+\lambda_2)t} + \left(\frac{2\lambda_2}{\lambda_1-\lambda'_1-\lambda_2} - \frac{\lambda_1}{\lambda'_1}\right)e^{-(\lambda_1+\lambda'_1+2\lambda_2)t} \quad (28)$$

Let $\lambda_1 = 0.001; \lambda'_1 = 0.0005, \lambda_2 = 0.0004, \mu_1 = \mu_1 = 0.05, \mu_2 = 0.10$, using these values, the reliability formula presented in (28) can be written as

$$R(t) = 3e^{-0.0018t} - 8e^{-0.0024t} + 6e^{-0.0023t} \quad (29)$$

Let $Q = \begin{bmatrix} -0.0023 & 0 & 0 \\ 0.0015 & -0.0018 & 0 \\ 0.0008 & 0 & -0.0024 \end{bmatrix}$

and take. T=4000 (hours), dt=100, t=0. The solution is carried out for $3-out-of-4:G$ warm standby system and Laplace transform solution (29) for different values of is presented in Table 1.

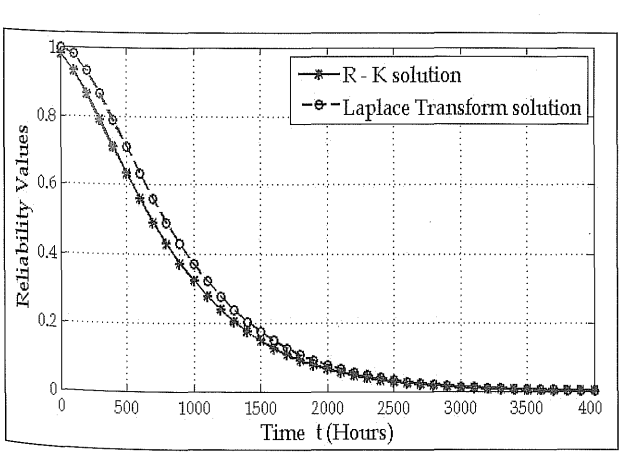

Fig. 5. Reliability values of Laplace Transform Technique versus R-K method

Table 2 List of all Failure rates 1-out-of-2, 1-out-of-3, 2-out-of-3 and 2-out-of-4, DG Configurations

S. No.	Failure rate	Values	Abbreviation
1	Q_{tr}	0.00291/h	Total failure rate of DG to run
2	Q_{ts}	0.03/d	Total failure probability of a DG to start
3	β_2	0.088	CCF parameter for system size 2
4	β_3	0.124	CCF parameter for system size 3
5	β_4	0.147	CCF parameter for system size 4
6	γ_3	0.420	CCF parameter for system size 3
7	γ_4	0.528	CCF parameter for system size 3
8	δ_4	0.505	CCF parameter for system size 3
9	λ_f	0.00265/h	failure rate of DG
10	λ_r	0.125/h	repair rate of DG
11	λ_{fwr}	0.00265/h	Failure to run rate of DG
12	λ_{ccfr}	0.25/h=0.25	Common cause failure
13	λ_{fwr22}	$\beta_2 \times Q_{tr}$ =0.00264	Failure to run rate of 2 out of 2 DG due to CCF
14	λ_{fwr23}	$(1-\gamma_3)\times\beta_3\times Q_{tr}/2$ =0.0001046436	Failure to run rate of 2 out of 3 DG due to CCF
15	λ_{fwr24}	$(1-\gamma_4)\times\beta_4\times Q_{tr}/3$ =0.00006730248	Failure to run rate of 2-out-of-4 DG due to CCF
16	λ_{fwr33}	$\gamma_3 \times \beta_3 \times Q_{tr}$ =0.0 001515528	Failure to run rate of 3-out-of-3 DG due to CCF
17	λ_{fwr34}	$(1-\delta_4)\times\gamma_4\times\beta_4\times Q_{tr}/3$ =0.000114060592	Failure to run rate of 3-out-of-4 DG due to CCF
18	λ_{fwr44}	$\delta_4 \times \gamma_4 \times \beta_4 \times Q_{tr}$ =0.000114060592	Failure to run rate of 4-out-of-4 DG due to CCF
19	P_{fts}	$(1-\beta)\times Q_{ts}$ =0.02 74	Probability that a DG fails to start
20	P_{fts22}	$\beta \times Q_{ts}$ =0.00264	Prob. of failure to start 2-out-of-2 DG due to CCF
21	P_{fts23}	$(1-\gamma_3)\times\beta_3\times Q_{ts}/2$ = 0.0001046436	Prob. of failure to start 2-out-of-3 DG due to CCF
22	P_{fts33}	$\gamma_3 \times \beta_3 \times Q_{ts}$ =0.00 15624	Prob. of failure to start 3-out-of-3 DG due to CCF
23	P_{fts24}	$(1-\gamma_4)\times\beta_4\times Q_{ts}/3$ = 0.00069384	Prob. of failure to start 2-out-of-4 DG due to CCF
24	P_{fts34}	$(1-\delta_4)\times\gamma_4\times\beta_4\times Q_{ts}/3$ = 0.0003841992	Prob. of failure to start 3-out-of-2 DG due to CCF
25	P_{fts44}	$\delta_4 \times \gamma_4 \times \beta_4 \times Q_{ts}$ = 0.0011758824	Prob. of failure to start 4-out-of-2 DG due to CCF

We note that the solution obtained using R-K method is closer to the Laplace solution for different values of time t. In Fig. 5, the solution obtained by R-K method and Laplace transform Technique are plotted.

6. Case Study: Markov Model for Estimating the Reliability and Unavailability of DG Configurations

In a NPP, in order to calculate the station blackout (SBO) frequency as a function of time, one should know the probability that the DG will be unavailable for a given interval of time [9]. For a single DG this can happen, either the DG failed to start or was not repaired in a given time interval. For 1-out-of-2:DG, 2-out-of-4:DG configurations there will be many possibilities which will lead to the unavailability of DG. Here 1-out-of-2:DG, 1-out-of-3:DG and 2-out-of-3:DG, 2-out-of-4:DG configurations are discussed and reliability obtained by R-K method the corresponding. Markov state transition diagram for

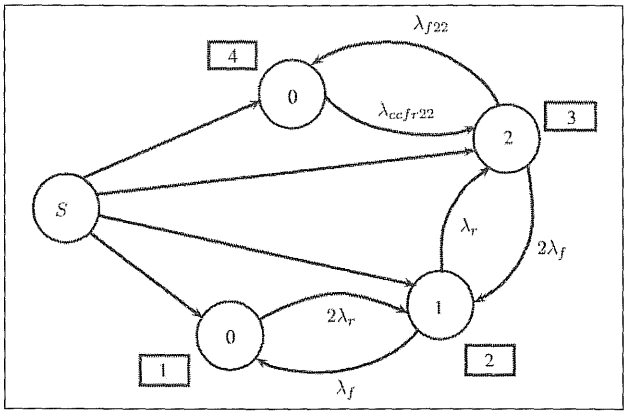

Fig.6. Markov state transition diagram for 1-out-of-2:DG configuration

these systems are shown in Fig. 6, Fig. 10 and Fig. 12 respectively. The number mentioned inside the circle denotes the number of DG that has not failed and *S* is the starting state and in all the DG configurations the Markov states are represented by rectangles.

The failure data used in the quantification of reliability and unavailability for 1-out-of-2, 1-out-of-3, 2-out-of-3, 2-out-of-4, DG configurations are presented in the Table 2 [9].

6.1 System Reliability Estimation of 1-out-of-2:DG Configuration

The state transition diagram for 1-out-of-2:DG configuration is shown Fig. 6.

The states of 2 DG configuration are converted into system of first order differential equations and the probability that the system is in state *i* at time is represented by the following equations

$$P_1(0) = P_{fts}^2 \tag{30}$$

$$P_2(0) = 2\times(1-P_{fts})P_{fts} \tag{31}$$

$$P_3(0) = \left[1-\sum_{i\neq 3} P_i(0)\right] \tag{32}$$

$$P_4(0) = P_{fts22} \tag{33}$$

The Markov transition matrix Q of 1-out-of-2:DG configuration is

$$Q = \begin{bmatrix} -2\lambda_r & \lambda_{fwr} & 0 & 0 \\ 2\lambda_r & -\lambda_r - \lambda_{fwr} & 2\lambda_{fwr} & 0 \\ 0 & \lambda_r & -2\lambda_{fwr} - \lambda_{fwr22} & \lambda_{ccfr} \\ 0 & 0 & \lambda_{fwr22} & -\lambda_{ccfr} \end{bmatrix}$$

Using Table 2, the above matrix Q is given by

Solving the first order differential equations, the system unavailability of 1-out-of-2:DG configuration is

$$U_{DG1/2}(t) = P_1(t) + P_4(t) \tag{34}$$

Reliability of 2 DG configuration is carried out by using R-K method presented in section 3. Now, Laplace transform technique of 1-out-of-2:DG is given by

$$Q = \begin{bmatrix} s+0.25 & -0.00265 & 0 & 0 \\ -0.25 & s+0.12765 & -0.0053 & 0 \\ 0 & -0.125 & s+0.005556 & -0.25 \\ 0 & 0 & -0.000256 & s+0.25 \end{bmatrix}$$

The reliability of the 1-out-of-2:DG configuration having initial probability vector for using Laplace transform technique is given by

Table 3 Reliability Values of R-K Method and Laplace Transform Technique for 1-out-of-2:DG Configuration

S. No	Time t Values	R-K Method solution	Laplace Transform Technique Solutions
1	0	0.9997	1.0000
2	0.5	0.9994	0.9997
3	1	0.9991	0.9994
4	1.5	0.9989	0.9991
5	2	0.9988	0.9989
6	2.5	0.9986	0.9987
7	3	0.9985	0.9986
8	3.5	0.9984	0.9984
9	4	0.9983	0.9983
10	4.5	0.9982	0.9982
11	5	0.9982	0.9982
12	5.5	0.9982	0.9981
13	6	0.9981	0.9980
14	6.5	0.9981	0.9980
15	7	0.9981	0.9979
16	7.5	0.9981	0.9979
17	8	0.9981	0.9979

$$R_{DG1/2}(t) = P_2(t) + P_3(t)$$
$$= 0.153377\, e^{-0.127974t} - 0.00392245\, e^{-0.245341t}$$
$$+0.0101042 e^{-0.259895t} + 0.0404412 - 0.152022 e^{-0.127974t}$$
$$-0.0154393\, e^{-0.245341t} + 0.0103534\, e^{-0.259895t}$$
$$+0.957108 \qquad (35-a)$$

The reliability values arrived using R–K. method and Laplace transform technique using (35-a) is presented in the following Table 3.

The reliability values for R–K method and Laplace transform technique are graphically shown below in Fig. 7.

The R–K method solutions are very closer to Laplace transform solutions as demonstrated in the above Fig. 7. The unavailability values are calculated using the equation (35-b) and presented in Table 4.

$$U_{DG1/2}(t) = P_1(t) + P_4(t)$$
$$= 0.00328858\, e^{-0.127974t} - 0.00214587\, e^{-0.245341t}$$
$$-0.0016329\, e^{-0.259895t} + 0.000490196$$
$$-0.001533\, e^{-0.127974t} + 0.00575369 e^{-0.245341t}$$
$$-0.00544618\, e^{-0.259895t} + 0.00122549 \qquad (35-b)$$

Table 4 Unavailability of R-K Method and Laplace Transform Technique Solutions for 1–out–of–2:DG Configuration

S. No	Time t Values	R-K Method solution	Laplace Transform Technique Solution
1	0	0.00033937	0.000000006
2	0.5	0.00062765	0.000337330
3	1	0.00087160	0.000624360
4	1.5	0.0011	0.000867950
5	2	0.0012	0.0011
6	2.5	0.0014	0.0012
7	3	0.0015	0.0014
8	3.5	0.0016	0.0015
9	4	0.0017	0.0016
10	4.5	0.0018	0.0017
11	5	0.0018	0.0018
12	5.5	0.0018	0.0018
13	6	0.0019	0.0019
14	6.5	0.0019	0.0019
15	7	0.0019	0.0019
16	7.5	0.0019	0.0020
17	8	0.0019	0.0020

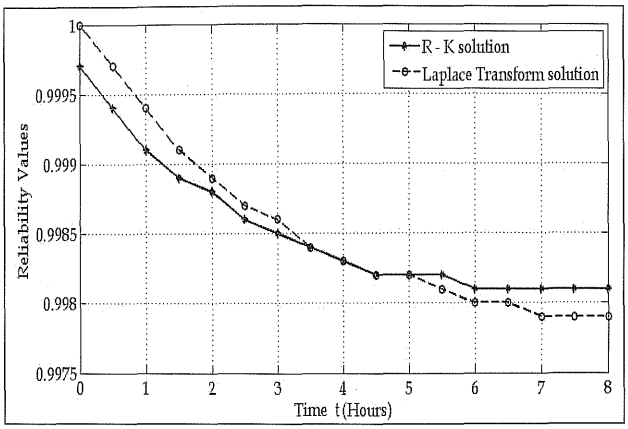

Fig. 7. Reliability values for R–K method and Laplace transform technique of 1–out–of–2:DG configuration

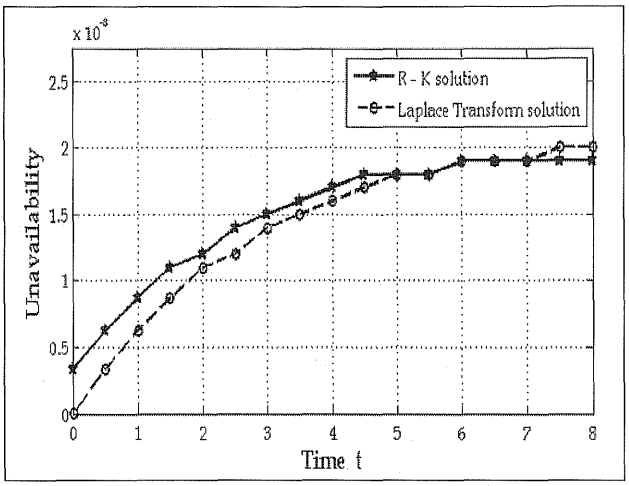

Fig. 8. Unavailability values for R-K method and Laplace Transform Technique solutions for 1–out–of–2:DG configuration

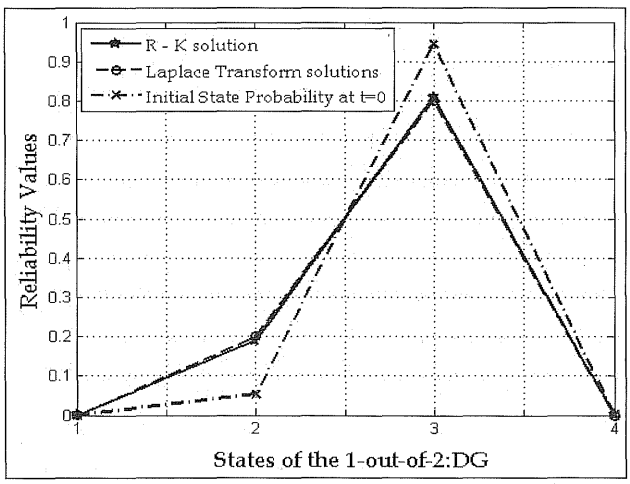

Fig. 9. Reliability values of R – K Method and Laplace Transform Technique solutions with initial state probability of each states at time t=0.

In Fig. 8. It can be observed that the unavailability values derived by the two methods are very closer for different values of time t as mentioned in the Table 4.

Table 5 Initial State Probability Values and R-K method, Laplace Transform Technique Solutions for 1-out-of-2:DG Configuration

S. No	R-K method Solutions	Laplace Transform Technique Solutions	Initial Markov state probability function t=0
1	0.0002	0.000000006	0.00075076
2	0.1897	0.2000	0.05329848
3	0.8099	0.8000	0.94331076
4	0.0001	0.0000	0.00264000

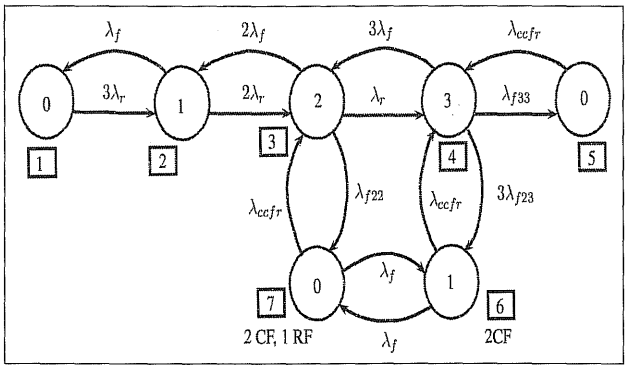

Fig. 10. Markov state transition diagram for 1-out-of-3 and 2-out-of-3:DG configurations

The R-K method, Laplace transform solutions are compared to the Markov initial state probability equations from (30)-(33) in Table 5 and graphically demonstrated in Fig. 9.

6.2 System Reliability Estimation of 1-out-of-3 and 2-out-of-3 DG Configuration

The state transition diagram for 3 DG configuration is shown in Fig. 10. The states involving CCF (for example. 2 CF, 1 RF means 2 DGs have failed due to a common cause and 1 due to independent) as shown in Fig. 10.

The states of the above transition diagram are converted into system of first order ordinary differential equations and the system is in state i at time is represented in the equations (36)-(42) below

$$P_1(0) = P_{fts}^3 \tag{36}$$

$$P_2(0) = 3 \times P_{fts}^2 \times (1 - P_{fts}) \tag{37}$$

$$P_3(0) = 3 \times P_{fts} \times (1 - P_{fts})^2 \tag{38}$$

$$P_4(0) = \left[1 - \sum_{i \neq 4} P_i(0)\right] \tag{39}$$

$$P_5(0) = P_{fts33} \tag{40}$$

$$P_6(0) = 3 \times P_{fts23} \times (1 - P_{fts}) \tag{41}$$

$$P_7(0) = 3 \times P_{fts22} \times P_{fts} \tag{42}$$

Using Table 2, the Markov transition matrix Q obtained based on the transition values is given by

Table 6 Reliability and Unavailability Values for R-K Method of 1-out-of-3:DG and 2-out-of-3:DG Configurations

S. No	Time t Values	Reliability Values of 1-out-of-3 DG	Unavailability Values of 1-out-of-3 DG	Reliability Values of 2-out-of-3 DG	Unavailability Values of 2-out-of-3 DG
1	0	0.9998	0.00009404	0.9985	0.0014
2	0.5	0.9996	0.00017399	0.9972	0.0025
3	1	0.9994	0.00024199	0.9962	0.0035
4	1 .5	0.9992	0.00029985	0.9952	0.0043
5	2	0.9990	0.00034912	0.9945	0.0049
6	2 .5	0.9988	0.00039107	0.9938	0.0054
7	3	0.9986	0.00042681	0.9933	0.0058
8	3 .5	0.9985	0.00045727	0.9928	0.0061
9	4	0.9983	0.00048322	0.9924	0.0064
10	4.5	0.9981	0.00050534	0.9921	0.0065
11	5	0.9979	0.00052420	0.9918	0.0066
12	5.5	0.9977	0.00054026	0.9916	0.0067
13	6	0.9976	0.00055395	0.9914	0.0067
14	6.5	0.9974	0.00056560	0.9912	0.0067
15	7	0.9972	0.00057552	0.9911	0.0067
16	7.5	0.9970	0.00058395	0.9910	0.0067
17	8	0.9968	0.00059112	0.9909	0.0067

$$Q=\begin{bmatrix} -0.375 & 0.00265 & 0 & 0 & 0 & 0 & 0 \\ 0.375 & -0.25265 & 0.0053 & 0 & 0 & 0 & 0 \\ 0 & 0.25 & -0.130556 & 0.00795 & 0 & 0 & 0.25 \\ 0 & 0 & 0.125 & -0.0088696 & 0.25 & 0.25 & 0 \\ 0 & 0 & 0 & 0.0001516 & -0.25 & 0 & 0 \\ 0 & 0 & 0 & 0.0003141 & 0 & -0.24735 & 0.125 \\ 0 & 0 & 0.000256 & 0 & 0 & 0.00265 & -0.375 \end{bmatrix}$$

Solving first order ordinary differential equations the system unavailability of 2 DG configuration is given by

$$U_{DG\,1/3}(t) = P_1(t) + P_5(t) + P_7(t) \quad (43)$$

$$U_{DG\,2/3}(t) = P_1(t) + P_2(t) + P_5(t) + P_6(t) + P_7(t) \quad (44)$$

Reliability of 1−out−of−3:DG and 2−out−of−3:DG configurations are carried out using R−K method having initial probability vector $P_i(0) = [0\ 0\ 0.5\ 0.5\ 0\ 0\ 0]^T$ for $i = 1,\cdots,7$ and unavailability computed from (43) and (44) are presented in Table 6.

The reliability and unavailability for 1−out−of−3: DG and 2−out−of−3:DG configurations are shown in Fig. 13 and Fig. 15 respectively.

The initial unavailability obtained from initial Markov probability state equations (36)-(42) based on Table 2, and the results of RK method is shown in Table 7.

Table 7 Initial State Probability Values and R-K Method for 1−out−of−2 and 2−out−of−3 DG Configuration

S. No	R-K Method	Initial Markov state probability function at t=0
1	0.0000	0.000020571
2	0.0012	0.002190657
3	0.4705	0.077757152
4	0.5280	0.915104579
5	0.0000	0.001562400
6	0.0001	0.003147723
7	0.0001	0.000217008

Fig. 11.shows the comparison of initial state probability values for each state derived using (36)-(42) and the results of R-K method for 1−out−of−3:DG and 2−out−of−3:DG configurations.

6.3 System Reliability Estimation of 2−out−of−4:DG Configuration

The state transition diagram for 4 DG configuration is shown in Fig. 12.

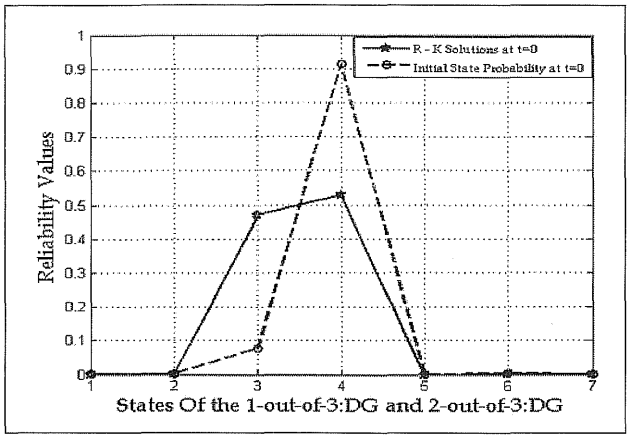

Fig. 11. Reliability values of R − K method with initial state probability of each states at time t=0.

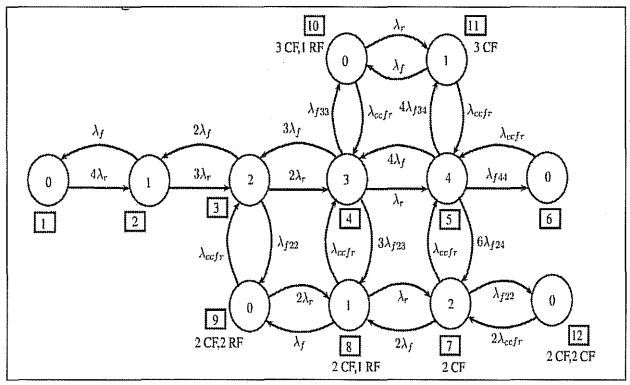

Fig. 12. Markov state transition diagram for 2−out−of−4:DG configuration

From Fig. 12. The 2−out−of−4:DG configuration is converted into system of first order differential equations and the Markov based initial state probability function is given by

The unavailability of 2−out−of−4:DG is given by

$$P_1(0) = P_{fts}^4 \quad (45)$$

$$P_2(0) = 4\times P_{fts}^3 \times (1-P_{fts}) \quad (46)$$

$$P_3(0) = 6\times P_{fts}^2 \times (1-P_{fts})^2 \quad (47)$$

$$P_4(0) = 4\times P_{fts} \times (1-P_{fts})^3 \quad (48)$$

$$P_5(0) = \left[1 - \sum_{i\neq 5} P_i(0)\right] \quad (49)$$

$$P_6(0) = P_{fts\,44} \quad (50)$$

$$P_7(0) = 6\times P_{fts\,24} \times (1-P_{fts})^2 \quad (51)$$

$$P_8(0) = 12\times P_{fts\,24} \times P_{fts} \times (1-P_{fts}) \quad (52)$$

$$P_9(0) = 6\times P_{fts\,24} \times P_{fts}^{\ 2} \quad (53)$$

$$P_{10}(0) = P_{fts} \times P_{fts\,34} \quad (54)$$

$$P_{10}(0) = P_{fts} \times P_{fts34} \quad (54)$$

$$P_{11}(0) = 4 \times P_{fts34} \times (1 - P_{fts}) \quad (55)$$

$$P_{12}(0) = 6 \times P_{fts24} \times P_{fts24} \quad (56)$$

$$U_{DG\,2/4}(t) = \sum_{i \neq 3,4,5,7} P_i(t) \quad (57)$$

Reliability of 2−out−of−4:DG configuration is carried out using R−K method presented in section 3. The reliability estimated using R-K using RK method having initial probability vector for and unavailability Values computed from (57) of 2−out−of−4:DG is shown in Table 8.

Table 8 Reliability and Unavailability of R-K Method for 2-out-of-4:DG Configuration

S. No	Time t Value	R-K Method solutions	Unavailability Values of 2-out-of-4 DG
1	0	0.9998	0.00016759
2	0.5	0.9997	0.00030765
3	1	0.9996	0.00042473
4	1.5	0.9995	0.00052261
5	2	0.9994	0.00060443
6	2.5	0.9993	0.00067283
7	3	0.9993	0.00072999
8	3.5	0.9992	0.00077774
9	4	0.9992	0.00081762
10	4.5	0.9991	0.00085090
11	5	0.9991	0.00087865
12	5.5	0.9991	0.00090177
13	6	0.9991	0.00092099
14	6.5	0.9991	0.00093696
15	7	0.9990	0.00095020
16	7.5	0.9990	0.00096114
17	8	0.9990	0.00097016

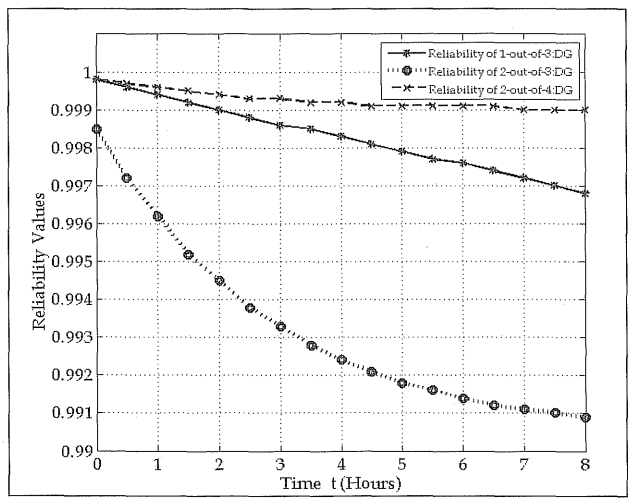

Fig. 13. Reliability values for 1−out−of−3:DG and 2−out−of−3:DG with 2−out−of−4 DG configurations

Using Table 8, the reliability values for 2−out−of−4:DG configuration along with the reliability values taken from Table 6 for 1−out−of−3: DG and 2−out−of−3:DGconfigurations are demonstrated in Fig. 13.

The initial reliability values obtained from initial Markov state probability equations (45)−(56) and results of R−K method is shown in Table 9.

Table 9 Initial State Probability Values and R-K Method for 2−out−of−4:DG Configuration

S. No	R-K Method solutions	Initial Markov state probability function t=0
1	0.0000	0.000000564
2	0.0006	0.000080029
3	0.2210	0.004261092
4	0.2637	0.100835475
5	0.2939	0.887975814
6	0.0000	0.001175882
7	0.2201	0.003938031
8	0.0006	0.000221884
9	0.0000	0.000003125
10	0.0000	0.000010527
11	0.0000	0.001494689
12	0.0000	0.000002888

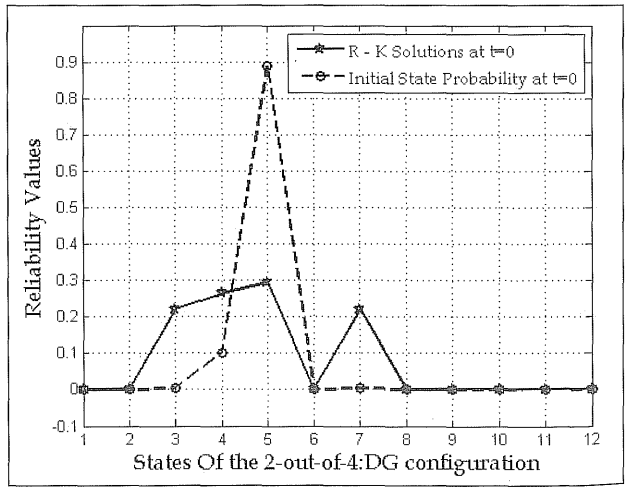

Fig. 14. Reliability values of R − K method with initial state probability of each states at time =0.

Fig. 14.shows at time t=0 zero, the initial state probability values for each state using (45)−(56) and compared to the results of R-K method for 2−out−of−4:DG configuration.

Using Table 8, the unavailability values for 2−out−of−4:DG configuration along with the unavailability values taken from Table 6 for

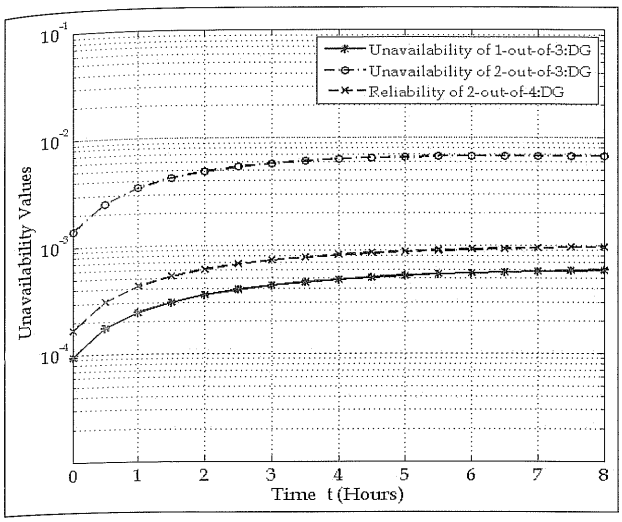

Fig. 15. Unavailability values for 1–out–of–3:DG, 2–out–of–3:DG with 2–out–of–4:DG configurations

1–out–of–3:DG and2–out–of–3:DG, configurations are shown in Fig. 15.

In Fig. 15, the unavailability values are gradually increasing for different time values.

7. Conclusions

In this paper, Laplace Transform Technique and of fourth order Runge-Kutta algorithm method is used to compute reliability for $3-out-of-4:G$ warm standby systems is discussed. Solutions obtained by these two methods indicate very a closer and similar solution, graphically shown in Fig. 5. The reliability estimation of 1–out–of–2:DG, 1–out–of–3:DG and 2–out–of–3:DG with 2–out–of–4:DG configurations are discussed thereby reliability is estimated using R–K method as graphically plotted in Fig 7, Fig 13. Analytic solutions of 1–out–of–2:DG configuration by Laplace transform technique solutions are carried out and compared to R–K method, these results are demonstrated graphically in Fig 7. The unavailability values of 1–out–of–2:DG configuration obtained from R–K method and Laplace transform technique is plotted in Fig. 8. Initial state probabilities equations at time t=0 is compared to the proposed R–K method and demonstrated in Fig. 9, Fig. 11 and Fig. 14. Onc can notice that the computation of analytic solutions for 1–out–of–3:DG or 2–out–of–3:DG and 2–out–of–4:DG configurations using Laplace transform technique is tedious as compared to R–K method. Thus, the reliability of 1–out–of–3:DG or 2–out–of–3:DG and 2–out–of–4:DG configurations using R–K method is plotted in Fig. 13 and its corresponding unavailability values are demonstrated in Fig. 15. Hence, the reliability computations based on the case study it can be observed the R–K method provides a computationally efficient solution as compared to Laplace transform technique. Finally in this paper, if the Markov transition diagram having more than 5 states then difficult to achieve the Laplace Transform techniques as observed in Figure 10 and Fig. 12 respectively. In this proposed method, the reliability and unavailability values of these systems are carried out by R–K method which depends on the initial state probability vector for any type of state dependent systems that obey the concept of Markov Chain.

Acknowledgement

The authors thank SSN management and Principal for their support.

References

1. Charles E. Ebeling, An Introduction to Reliability and Maintainability Engineering, Tata McGraw-Hill Edition, Fourteenth Reprint,2011.
2. Kishor S. Trivedi, Probability & Statistics with Reliability, Queuing and Computer Science Applications, Second Edition, John Wiley & Sons, 2002.
3. Lirong Li, and Xiaoyue Wu, "Runge–Kutta Algorithm of Reliability Model Based on Markov Chain for TT&C System," J. Math. Analysis and Applications, vol. 57, pp. 299–303, 2011.
4. Roy Billinton, Ronald N. Allan, Reliability Evaluation of Engineering Systems:Concepts and Techniques, 2nd ed., Springer International Edition, 2008.
5. Zhang Xiaonan, Liu Anxin, Gao Yaming, Zhang Tiefu, and Liu Hongliang, "The Prediction Model of Software Reliability Based on the Modular," IEEE–International Forum on Information Technology and Applications, 2, pp. 315–318.
6. Sujatha R, Boopathi M, and Senthil Kumar C, "Reliability Estimation of State Dependent Systems Using Fourth Order Runge–Kutta Algorithm," International Conference on Mathematical Computer Engineering:ICMCE–2013, pp.734-739, 2013.
7. Zhang TL, and Horigome M. Availability of 3–out–of–4:DG Warm Standby System. IEICE Trans Fundam. Electron. Commun. Comput. Sci; E83-A(5), pp. 857–862, 2000.
8. Tieling Zhang, Min Xie, and Michio Horigome, "Availability and Reliability of Warm Standby Systems," Reliability Engineering & System Safety,Volume 91, Issue 4, pp.381–387, April 2006.
9. Senthil Kumar C, John Arul A, Marimuthu S, Om Pal Singh, New Methodologies for Station Blackout Studies in Nuclear Power Plant, Reliability, Safety and Hazard, Narosa Publishing House, New Delhi, India, pp. 331–338, 2006.

Guidelines for Preparing the Manuscript

A softcopy of the complete manuscript should be sent to the Chief-Editors by email at the address: editor@sresa.org.in. The manuscript should be prepared using 'Times New Roman' 12 font size in double spacing, on an A-4 size paper. The illustrations and tables should not be embedded in the text. Only the location of the illustrations and tables should be indicated in the text by giving the illustration / table number and caption.

The broad structure of the paper should be as follows: a) Title of the paper – preferably crisp and such that it can be accommodated in one or maximum two lines with font size of 14 b) Name and affiliation of the author(s), an abstract of the paper in ~ 100 words giving brief overview of the paper and d) Five key words which indicates broad subject category of the paper. The second page of the paper should start with the title followed by the Introduction

A complete postal address should be given for all the authors along with their email addresses. By default the first author will be assumed to be the corresponding author. However, if the first author is not the corresponding author it will be indicated specifically by putting a star superscript at the end of surname of the author.

The authors should note that the final manuscript will be having double column formatting, hence, the size of the illustration, mathematical equations and figures should be prepared accordingly.

All the figures and tables should be supplied in separate files along with the manuscript giving the figure / table captions. The figure and table should be legible and should have minimum formatting. The text used in the figures and tables should be such that after 30% reduction also it should be legible and should not reduced to less than font 9.

Last section of the paper should be on list of references. The reference should be quoted in the text using square bracket like '[1]' in a chronological order. The reference style should be as follow:

1. Pecht M., Das D, and Varde P.V., "Physics-of-Failure Method for Reliability Prediction of Electronic Components", Reliability Engineering and System Safety, Vol 35, No. 2, pp. 232- 234, 2011.

After submitting the manuscript, it is expected that reviews will take about three months; hence, no communication is necessary to check the status of the manuscript during this period. Once, the review work is completed, comments, will be communicated to the author.

After receipt of the revised manuscript the author will be communicated of the final decision regarding final acceptance. For the accepted manuscript the author will be required to fill the copy right form. The copy right form and other support documents can be down loaded from the SRESA website: http://www.sresa.org.in

Authors interested in submitting the manuscript for publication in the journal may send their manuscripts to the following address:

Society for Reliability and Safety
RN 68, Dhruva Complex
Bhabha Atomic Research Centre,
Mumbai – 400 085 (India)
e-mail : editor@sresa.org.in

The Journal is published on quarterly basis, i.e. Four Issues per annum. Annual Institutional Subscription Rate for SAARC countries is Indian Rupees Ten Thousand (Rs. 10,000/-) inclusive of all taxes. Price includes postage and insurance and subject to change without notice. For All other countries the annual subscription rate is US dollar 500 ($500). This includes all taxes, insurance and postage.

Subscription Request can be sent to SRESA Secretariat (please visit the SRESA website for details)

SRESA's International Journal of

Life Cycle Reliability and Safety Engineering

Contents

Vol. 5 Issue No.2 April-June 2016 ISSN – 2250 0820